AD NUMBER

ADB008416

LIMITATION CHANGES

TO:

Approved for public release; distribution is unlimited.

FROM:

Distribution authorized to U.S. Gov't. agencies only; Test and Evaluation; NOV 1975. Other requests shall be referred to Rome Air Development Center, Attn: OCTM, Griffiss AFB, NY 13441.

AUTHORITY

RADC ltr, 14 Apr 1980

RADC-TR-75-303
Technical Report
November 1975

COAT MEASUREMENTS AND ANALYSIS

Hughes Research Laboratories

Sponsored by
Defense Advanced Research Projects Agency
ARPA Order No. 1279

Distribution limited to U. S. Gov't agencies only; test and evaluation; November 1975. Other requests for this document must be referred to RADC (OCTM), Griffiss AFB NY 13441.

The views and conclusions contained in this document are those of the authors and should not be interpreted as necessarily representing the official policies, either expressed or implied, of the Defense Advanced Research Projects Agency or the U. S. Government.

Rome Air Development Center
Air Force Systems Command
Griffiss Air Force Base, New York 13441

This report has been reviewed and is approved for publication.

APPROVED: Robert F. Ogrodnik

ROBERT F. OGRODNIK
Project Engineer

Do not return this copy. Retain or destroy.

COAT MEASUREMENTS AND ANALYSIS

J. E. Pearson
W. P. Brown
S. A. Kokorowski
M. E. Pedinoff
C. Yeh

Contractor: Hughes Research Laboratories
Contract Number: F30602-75-C-0001
Effective Date of Contract: 2 July 1974
Contract Expiration Date: 30 June 1975
Amount of Contract: $316,766.00
Program Code Number: 5E20
Period of work covered: Jan 75 - Mar 75

Principal Investigator: J. E. Pearson
213 456-6411 x283

Project Engineer: Robert F. Ogrodnik
315 330-4306

This research was supported by the Defense Advanced Research Projects Agency of the Department of Defense and was monitored by Robert F. Ogrodnik (OCTM), Griffiss Air Force Base, New York 13441.

UNCLASSIFIED
SECURITY CLASSIFICATION OF THIS PAGE (When Data Entered)

REPORT DOCUMENTATION PAGE

READ INSTRUCTIONS BEFORE COMPLETING FORM

1. REPORT NUMBER: RADC-TR-75-303	2. GOVT ACCESSION NO.
3. RECIPIENT'S CATALOG NUMBER	
4. TITLE (and Subtitle): COAT MEASUREMENTS AND ANALYSIS	5. TYPE OF REPORT & PERIOD COVERED: Qtrly Technical Report 3, Jan 75 - 31 March 1975
	6. PERFORMING ORG. REPORT NUMBER: N/A
7. AUTHOR(s): J. E. Pearson, W. P. Brown, S. A. Kokorowski, M. E. Pedinoff and C. Yeh	8. CONTRACT OR GRANT NUMBER(s): F30602-75-C-0001, ARPA Order-1279
9. PERFORMING ORGANIZATION NAME AND ADDRESS: Hughes Research Laboratories, 3011 Malibu Canyon Road, Malibu CA 90265	10. PROGRAM ELEMENT, PROJECT, TASK AREA & WORK UNIT NUMBERS: 12790017, AF-1279
11. CONTROLLING OFFICE NAME AND ADDRESS: Defense Advanced Research Projects Agency, 1400 Wilson Blvd, Arlington VA 22209	12. REPORT DATE: November 1975 (66 p.)
	13. NUMBER OF PAGES: 65
14. MONITORING AGENCY NAME & ADDRESS (if different from Controlling Office): Rome Air Development Center (OCTM), Griffiss AFB NY 13441	15. SECURITY CLASS. (of this report): UNCLASSIFIED
	15a. DECLASSIFICATION/DOWNGRADING SCHEDULE: N/A

16. DISTRIBUTION STATEMENT (of this Report)

Distribution limited to U. S. Gov't agencies only; test and evaluation; November 1975. Other requests for this document must be referred to RADC (OCTM), Griffiss AFB NY 13441.

17. DISTRIBUTION STATEMENT (of the abstract entered in Block 20, if different from Report)

Same Quarterly technical rept. 3, Jan - 31 Mar 75,

18. SUPPLEMENTARY NOTES

RADC Project Engineer:
Robert F. Ogrodnik (OCTM)

19. KEY WORDS (Continue on reverse side if necessary and identify by block number)

COAT, Optical Radar, Laser Phased Arrays, Thermal Blooming Compensation, Active Optics, Adaptive Systems, Target Signature Effects

20. ABSTRACT (Continue on reverse side if necessary and identify by block number)

Several propagation problems have been investigated using multidither Coherent Optical Adaptive Techniques (COAT). Multidither tracking and focus controls have been implemented into a computer simulation and into the DARPA/RADC experimental COAT model which previously had only 18 channels of planar phase control. Compensation for turbulence has been demonstrated both analytically and experimentally using these new controls. COAT-system/target-signature interaction effects have been studied experimentally and analytically. The (Cont'd)

over

DD FORM 1 JAN 73 1473 EDITION OF 1 NOV 65 IS OBSOLETE

UNCLASSIFIED
SECURITY CLASSIFICATION OF THIS PAGE (When Data Entered)

172600 net

experimental results indicate that the deleterious effects of target-induced speckle modulations are not as serious as suggested by earlier work. Computer simulation studies tend to support this observation, but are limited by inadequate knowledge of the amplitude and frequency spectrum of speckle modulations produced by realistic targets. Experimental thermal blooming studies in scaled laboratory experiments have shown a 35% improvement in peak target irradiance. Computer simulation studies of thermal blooming indicate that a "return-wave" COAT system may reduce the target irradiance under strong blooming, but this cannot occur with an irradiance maximization technique such as outgoing-wave multidither COAT.

TABLE OF CONTENTS

LIST OF ILLUSTRATIONS

PREFACE

This quarterly report was prepared by Hughes Research Laboratories, Malibu, California under Contract F30602-75-C-0001. It describes work performed from 1 January 1975 to 31 March 1975. The principal investigator and principal scientist is Dr. James E. Pearson. The project is part of the adaptive optics program in the Optoelectronics Department, managed by Dr. Viktor Evtuhov, at the Hughes Research Laboratories.

SUMMARY

The objectives of this research program are threefold: (1) to experimentally study the ability of a multidither COAT system to compensate for thermal blooming and turbulence, particularly when it operates against complex, multiple-glint targets; (2) to use computer simulation to cross check the experimental results and to investigate areas beyond the capabilities of the experimental hardware; and (3) to perform preliminary studies of the effects of speckle noise modulation on COAT system convergence and performance. This report summarizes the work performed during the third quarter of the contract from 1 January 1975 to 31 March 1975.

We have experimentally studied the effects of target motion-induced speckle modulation on the DARPA/RADC COAT system. A scaled laboratory experiment using a rotating scotchlite target produced a wideband speckle noise spectrum over the dither frequency band which did not observably interfere with the convergence properties of the system. In another series of experiments, an acousto-optic modulator with 64% modulation efficiency was placed in the DARPA/RADC COAT optical system and swept over a variable frequency bandwidth in a time comparable to the servo loop convergence time. The speckle modulation artificially generated by this technique produced interference signals over the dither band greater than the normal dither signals, and produced converged power degradation of 35%. The results obtained thus far indicate that the system performance can be significantly degraded if the modulation is large enough, but the systematic evaluation of which targets, target ranges, and target motions, if any, can actually produce such large modulations will be pursued on another program.

Computer simulation modeling of COAT system performance in the presence of speckle noise modulation has been used to obtain the average convergence level of an 18-channel multidither COAT system in the presence of this noise. An oscillation of the system about the average convergence level has been observed. A statistical analysis of the COAT system and of the speckle noise has been developed for use in explaining the simulation results.

Multidither adaptive tracking and focus (Beam Active Track or BAT) controls have been implemented into the DARPA/RADC COAT system and into a computer simulation code. The experimental tracking controls have demonstrated a convergence time of 8 to 10 msec, the design goal. A tendency for this system to lock onto sidelobes of the transmitter array has been observed. This behavior can be explained in terms of the sidelobes of the 18-element COAT planar array and in terms of the tracking dither frequency being larger than the open-loop bandwidth of the phase-control servo. The BAT computer simulation uses 2-axis tracking and 2-axis focusing (2 separately controlled cylindrical lenses). For moderate turbulence ($C_N^2 Z = 4.6 \times 10^{-11}\ m^{1/3}$), the BAT simulation shows an improvement in average strehl ratio from 0.67 to 0.86. For strong turbulence ($C_N^2 Z = 21 \times 10^{-11}\ m^{1/3}$), the improvement is from 0.2 to 0.5. Almost all of this improvement can be produced by the 2-axis focus controls alone; adding the tracking controls to the 2-axis focus provides only a small increase in strehl ratio. A 37-channel multidither COAT system achieves strehl ratios of 0.95 and 0.76 for these two turbulence levels.

Experimental observations with artificial turbulence equivalent to $C_N^2 Z = 5 \times 10^{-11}\ m^{1/3}$ have shown good agreement with the simulation data. We have observed an improvement in strehl ratio from 0.65 to 0.87 using only the tracking controls. When the 18-channel phase controls are also used, the strehl ratio increases to 0.95.

A flowing gas cell has been built and tested for thermal blooming studies. With the absorption region occurring in the last 81% of the focused propagation path, the 18 phase controls plus two-axis tracking controls produced a 35% increase in peak target irradiance. This correction is still less than expected and further study is indicated.

An exact simulation of both a multidither servo and time-dependent thermal blooming has been determined to be very costly, so no such computer runs have been made. We have shown that finite size target glints together with return-wave COAT systems can reduce, rather than increase target irradiance in the presence of blooming. These effects are not expected to be important with outgoing-wave multidither COAT systems (such as the DARPA/RADC system).

During the final contract quarter, work will be concentrated on experimental measurements of simultaneous thermal blooming and turbulence. Analytical work will focus primarily on comparing computer simulation results on speckle-modulation effects to experimental observations and on using the statistical models we have developed to explain the observations.

I. INTRODUCTION

A. Program Objectives

There are two primary objectives of this program. The first objective is to determine the performance limits of multidither coherent optical adaptive techniques (COAT) by performing scaled laboratory experiments which are designed to produce quantitative data on the nature of thermal blooming and turbulence and on the ability of multidither COAT to correct for these distortions, particularly when the target has many moving, time-varying glints. The second objective is to use computer simulation as a cross check on the experiments and as an analytical tool to extend the understanding of propagation distortions and of COAT systems beyond the capabilities of the experimental hardware.

B. Research Program Plan

The performance of multidither COAT has already been proved with an 18-element visible wavelength system developed and tested on DARPA/RADC Contract F30602-73-C-0248 which was concluded in July 1974. This same system is used for the laboratory experiments in this program. The computer simulation codes for atmospheric turbulence, thermal blooming, and the COAT system are being developed on DARPA/NOL Contract N60921-74-C-0249. The previous DARPA/RADC COAT contract also supplied a design for a gas absorption cell which has been used to simulate convection-dominated thermal blooming in the atmosphere.

The research program for this contract, illustrated in Fig. 1, runs from 2 July 1974 through 30 June 1975. The required oral presentation was made on 3 December 1974 as part of the DARPA/NOL Adaptive Optics Symposium held at Lincoln Laboratories.[1] A contract amendment negotiated during the second contract quarter provided for the addition of auto-tracking and autofocus controls to both the DARPA/RADC COAT hardware and the Naval Ordnance Laboratories computer code. A second amendment, negotiated during the third quarter, eliminated a high-power design guidelines task so that time and funds could be directed toward experiments on COAT/target-signature interactive effects. The schedule in Fig. 1 reflects these changes.

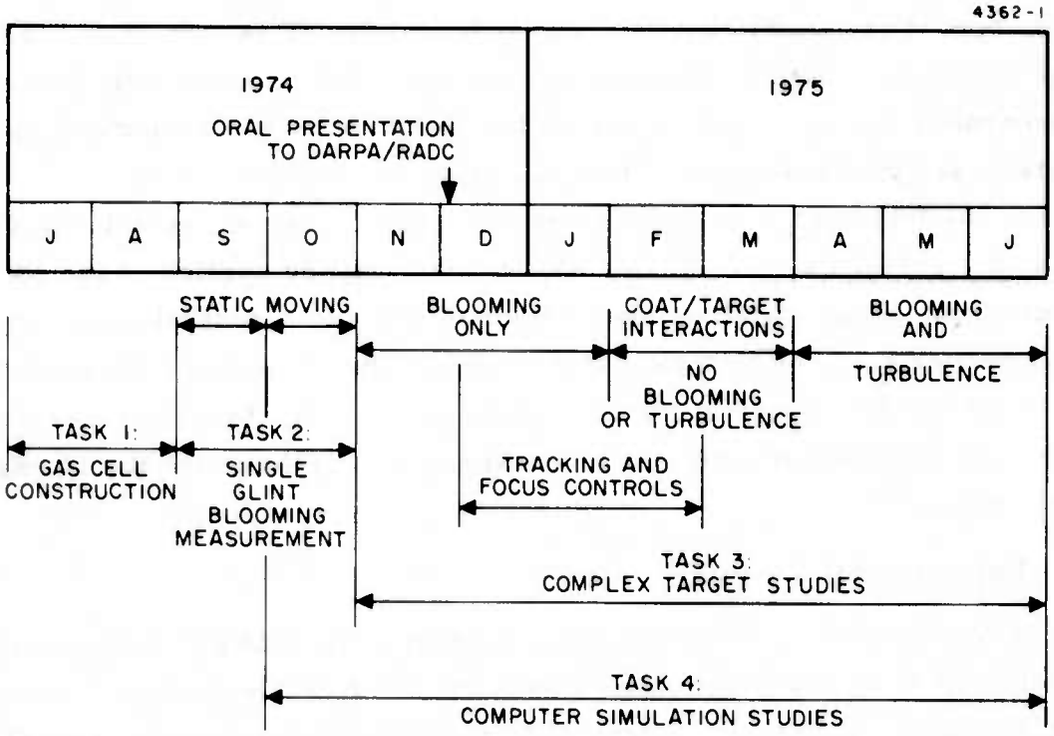

Fig. 1. Revised research program plan showing COAT tasks and scheduling.

II. TECHNICAL ACCOMPLISHMENTS

A. Adaptive Tracking and Focus Controls

Contract Amendment No. 1 provides for supplemental funding from the Air Force Weapons Laboratory to add multidither tracking and focus controls both to the DARPA/RADC experimental COAT hardware and to the Hughes multidither COAT computer simulation. The controls will be used both separately and in conjunction with the DARPA/RADC 18-channel phase controls to study turbulence and thermal blooming compensation.

In the following discussions, we will refer to three possible COAT system configurations. The term "18-channel" will be applied to the 18-element planar array which produces piston-type phase control on 18 separate transmitted beam segments. The acronym "BAT" (defined below) will apply to the new tracking and focus controls alone. The term "21-channel" will be used whenever the BAT controls are used together with the 18 phase control channels.

1. Experimental Results

A multidither tracking and focus control system has at various times been referred to by many names: "Conical Scan" (tracking only), "Beam Active Tracking" (BAT), or "Adaptive Laser Optical Techniques" (ALOT). For simplicity, we will refer to the controls developed here as BAT. The three-channel BAT system built for the DARPA/RADC COAT system is shown in Fig. 2. The tracking controls are designed to have a 50 Hz open-loop unity gain bandwidth and a 10 msec convergence time. They use two dither frequencies at 750 Hz and 1000 Hz or a single dither at 1000 Hz, with the sine signal applied to one channel and the cosine to the other (conical scan). The focus channel is a factor of 10 slower using a 100 Hz dither and designed to converge in 100 msec (5 Hz unity gain bandwidth).

The focus control shown in Fig. 3 uses a single piezoelectric (PZT) cylinder to deform a single mirror into a spherical shape. The unit was designed to use a 2.25 in. long PZT5-H cylinder and to have a loaded deflection sensitivity of 250 V/μm. We have been unable to obtain PZT5-H in the desired dimensions and so have used PZT-4. With this material, a deflection sensitivity of 520 V/μm is expected.

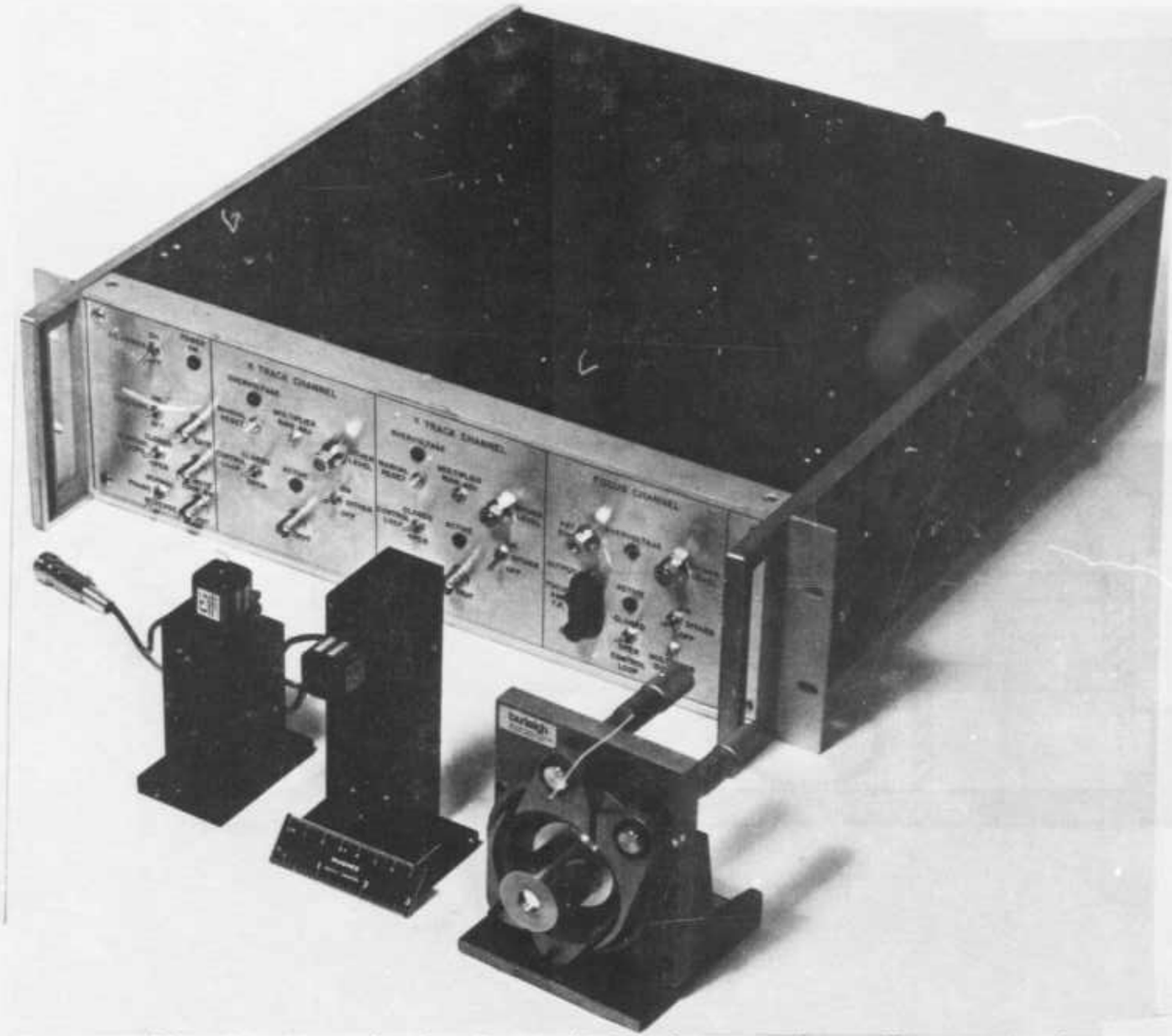

Fig. 2. Beam Active Track (BAT) focus and tracking controls

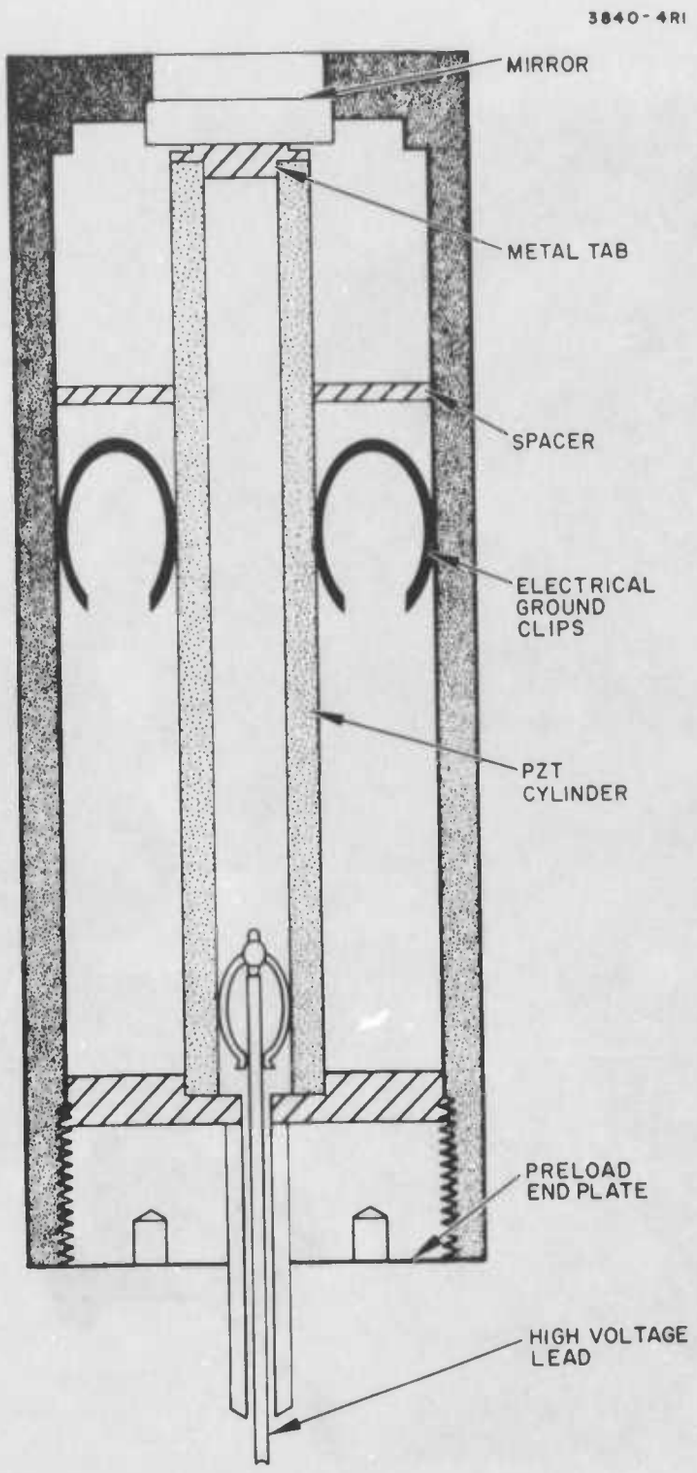

Fig. 3.
Piezo-electrically-driven, variable-radius spherical mirror used for autofocus control.

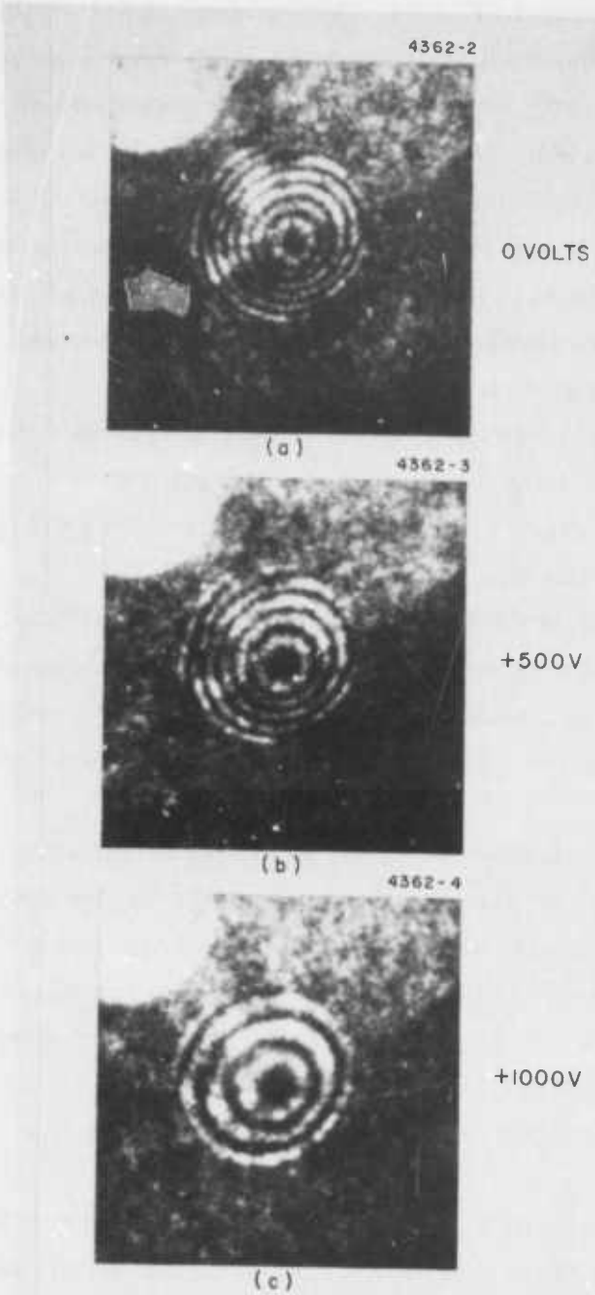

Fig. 4.
Static deflection tests of
BAT focus actuator

Static deflection tests of the focus actuator in a Twyman-Green interferometer are shown in Fig. 4. The observed deflection is quite uniform and spherical. The observed sensitivity is 1260 V/μm, a factor of 2.4 lower than the design value. We are not sure why the observed sensitivity is so much lower than expected. One possibility is that the mirror spring constant is larger than our calculations predicted relative to the PZT spring constant. The initial curvature (V = 0) is an adjustable preload on the PZT cylinder to provide a spring for the actuator to work against and to eliminate the need for a bond between the cylinder and the mirror. The lowest resonant frequency of this device was determined to be 3.4 kHz.

Because of some difficulties in the COAT system optics, we have not used the focus actuator in the system yet. During the next quarter we expect to resolve these difficulties so that the calibration and propagation tests with this device can be completed.

The tracking controls have been tested with the COAT system and some preliminary blooming compensation studies are reported in Section II-C. The lowest resonance of the galvanometer-plus-mirror combination is at 1.7 kHz. The convergence time shown in Fig. 5 is 8 to 10 msec, the design goal.

The tracking performance of the controls is shown in Fig. 6. An interesting behavior is observed: the controls do not automatically steer the beam boresight axis onto the glint when the phase and BAT controls are used together. The stable lock position depends on the initial conditions as shown in the figures. This behavior is not entirely reproducible and was not expected, but we now understand why it occurs; it is a consequence of the sidelobe structure of the segmented aperture and of the choice of dither frequencies.

To understand the multiple-state convergence of the BAT tracking controls, consider the diagrams in Fig. 7, showing the element and array patterns at the target plane. With no pointing/tracking control, the element pattern is fixed, and the COAT system adjusts the array pattern to maximize energy on the glint; the dotted line in Fig. 7 shows the array pattern and a sidelobe for a glint at point A. What the observations in Fig. 6 indicate is that if a glint is placed at point A with the tracking controls (BAT) off, and then the BAT system is turned on, the boresight axis is not steered to

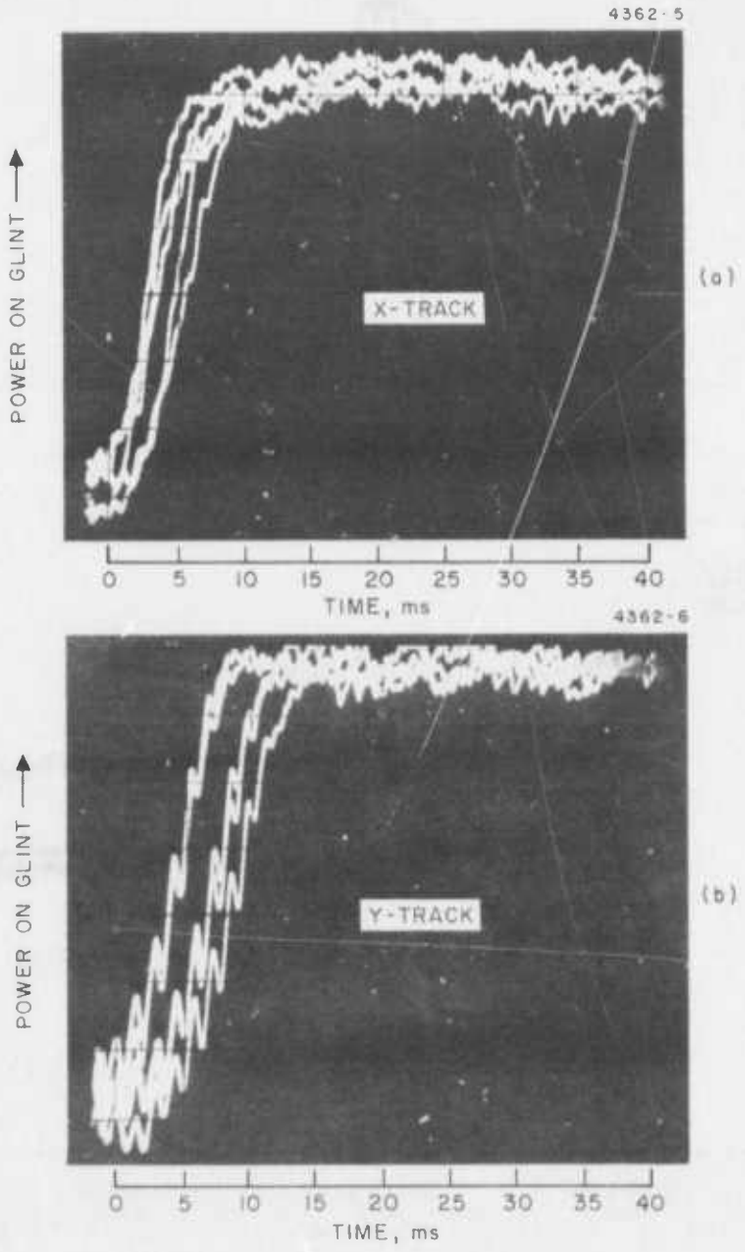

Fig. 5
Measured Convergence time
of BAT tracking controls

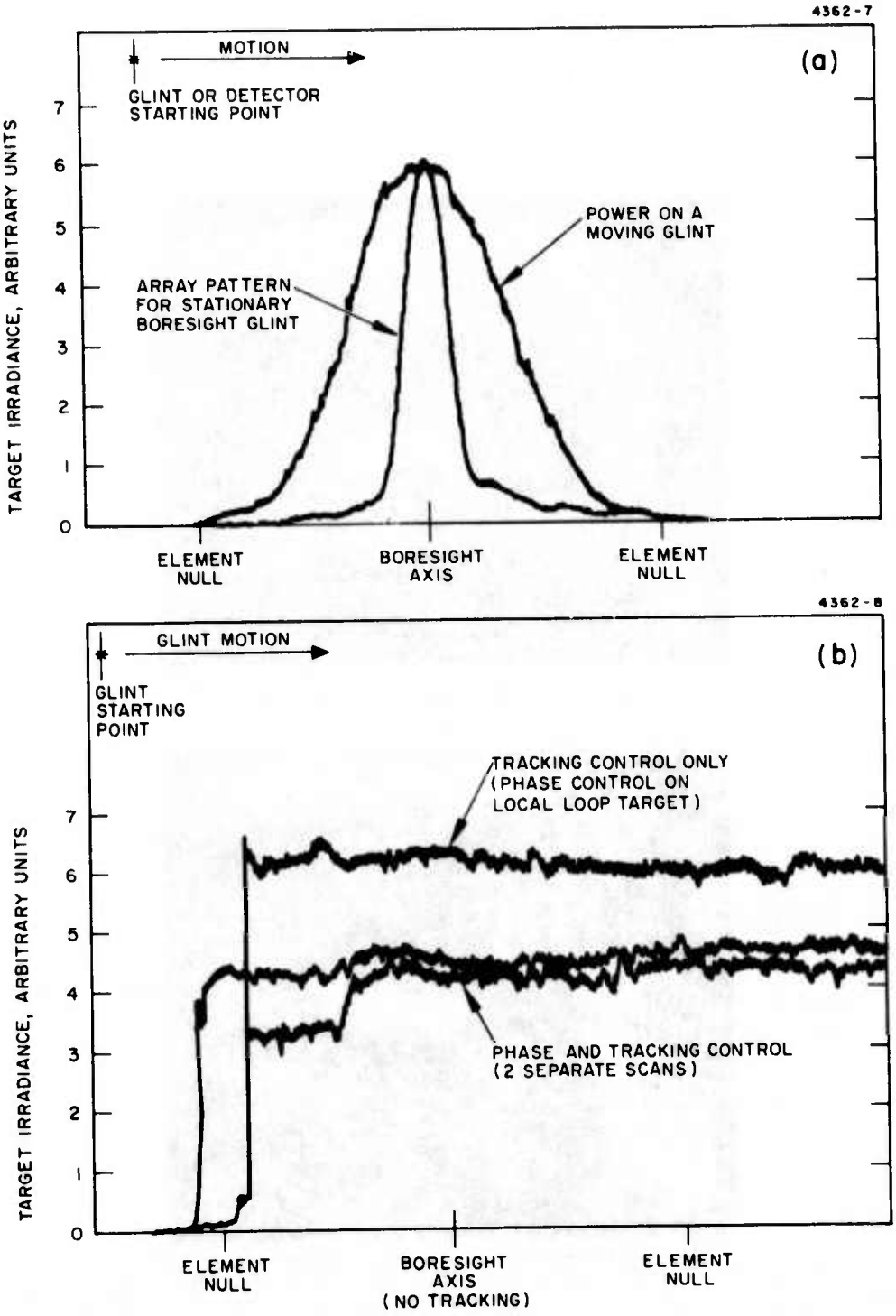

Fig. 6.
Tracking performance of COAT controls. (a) Tracking control off. The formed array pattern is also shown for reference. (b) Tracking control performance. Curves with tracking control only and with both phase and tracking controls are shown. The ability of the system to lock in a nonoptimum, off-boresight condition is evident.

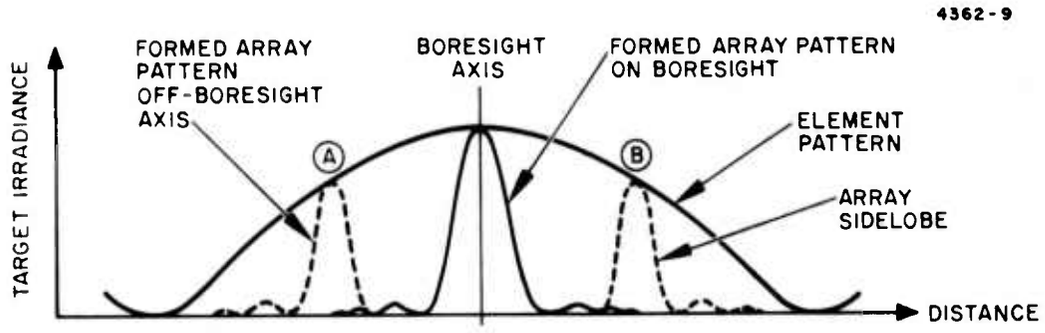

Fig. 7. Target intensity patterns produced by a segmented aperture, "piston-control," COAT system.

point A as we would like. The array pattern structure is maintained and the BAT system steers the element pattern as the glint moves. This type of behavior will not occur with a deformable mirror COAT system (or if the segmented aperture has element tilt as well as "piston" control), since the deformable mirror itself can tilt the "element" pattern and since a deformable mirror does not produce a side-lobe structure like a segmented array does.

This behavior is also a consequence of the choice of BAT dither frequency and is related to the servo loop gain. Intuitively, we can understand what is happening by noting that the servo loop gain is proportional to the change in target intensity with respect to beam motion, and therefore to the slope of the intensity pattern. If the BAT tracking dither is fast enough that the phase control cannot follow it, then the array pattern is fixed and it is the slope of the array intensity pattern that determines the maximum loop gain. On the other hand, if the BAT controls dither slowly, the COAT phase controls will reform the array pattern so that it is the slope of the element intensity pattern that is sensed. The latter case is what is necessary for boresighting to occur.

It is easy to show this result mathematically by approximating the total intensity pattern by

$$I(x) = \operatorname{sinc}^2\left(\frac{2\pi x}{D_e}\right) \operatorname{sinc}^2\left[\frac{2\pi x}{D_a} - \phi_c\left(1 - e^{-\omega_c t}\right)\right] \qquad (1)$$

where D_e and D_a are the element and array peak-null distances, $\omega_c = 1/\tau_c$ for τ_c the 10% to 90% convergence time of the COAT phase controls, and $\operatorname{sinc} u = \sin u/u$. By definition, the COAT system acts to produce $\phi_c = 2\pi x/D_a$. The BAT tracking dither around $x = 0$ is $x = A\sin\omega t$ and $\operatorname{sinc}^2 u = \sin^2 u/u^2 \simeq 1 - u^2/6$.

The maximum loop gain, G_m, is found from

$$G_m \propto \left(\frac{dI}{dt}\right)_{max} \qquad (2)$$

There are two cases to consider. First, when the BAT dither at ω is faster than the phase servo response (ω_c), Eqs. (1) and (2) give

$$(G_m)_{\omega \gg \omega_c} \approx \frac{\omega}{6}\left(\frac{2\pi A}{D_a}\right)^2 \quad . \tag{3}$$

When $\omega << \omega_c$,

$$(G_m)_{\omega << \omega_c} \approx \frac{\omega}{6}\left(\frac{2\pi A}{D_e}\right)^2 \quad . \tag{4}$$

The ratio of these two cases is D_e^2/D_a^2, which is 25 for the DARPA/RADC 18-element COAT array. The first case (Eq. (3)) is appropriate for the 1 kHz BAT dither now in use. This means that the loop gain for sensing the element pattern slope (Eq. (4)) is 25 times lower than that which senses the array pattern slope and which sets the BAT servo maximum loop gain. The maximum servo loop gain for low frequencies is about 35 dB; a factor of 25 lower corresponds to only 7 dB. This small loop gain is not enough to consistently drive the system to a boresighted condition, although boresighting will occur occasionally as indicated in Fig. 6.

Use of a 200 to 300 Hz dither would eliminate this behavior, but it would also produce a slower tracking system by a factor of 3 to 5. We have not yet demonstrated it, but we expect that disturbing effects such as turbulence or defocus will somewhat alleviate the problem and cause the BAT tracker to boresight with greater consistency even with the 1 kHz dither.

As a final result, we note that we have observed glint tracking, black-hole tracking, and edge tracking with this system. Except for the ineffective boresighting, no other unexpected behavior has been observed.

2. Computer Simulation Results

The BAT tracking and focus controls have been implemented into a multidither computer simulation that uses a deformable mirror as a dither and corrector element. The nonboresighting effects seen in the experiment were thus not observed. We also decided to implement a two-axis focus control, in effect using two cylindrical lens controls that focus along orthogonal axes. This type of focusing should be particularly useful with thermal

blooming since the negative thermal lens is much stronger perpendicular to the wind direction than parallel to it. The computer simulation is shown schematically in Fig. 8.

The computer simulation results have shown the expected 10 msec convergence time for the tracking controls and 100 msec for the focus. With the focus control, however, we observed another initially unexpected result: the final converged level depends on the magnitude of the initial defocus. This behavior is now understood to be a generalized manifestation of the "$2n\pi$ problem" encountered with deformable mirror COAT systems.

The behavior of the focus control can be understood by referring to Fig. 9. Figure 9(a) illustrates the well-known behavior[2] of the on-axis intensity of a focused beam: as the focal point is approached from either direction, the on-axis intensity goes through several maxima and minima. Each maxima away from the focal plane corresponds to a different Fresnel zone, or a $2n\pi$ phase difference between rays originating from the center of the focusing lens and the outer edge. If the initial defocus is at a point such as A in Fig. 9(a), the BAT focus control will drive the focus toward the maximum on-axis intensity. If the starting point is at B, however, the BAT multidither servo moves toward the nearest maximum at C and a nonoptimum target intensity results. Figure 9(b) shows several computer runs exhibiting this type of behavior.

The results shown in Fig. 9(b) exhibit an unusual behavior when the initial defocus is very large. The one run showing several oscillators, and achieving only 48% convergence at 14 μsec is particularly hard to understand. When longer run times for this case are used, we observe that the convergence level continues to increase, but very slowly. We do not understand this behavior at this time, but we expect that is a computational artifact rather than what will be observed in an experimental system. One possible explanation (which has not been verified but which we have some evidence for) is that the $2n\pi$-error sensing and removing routine built into the deformable mirror simulation may be cuasing the problem. The defocus error may be large enough that 2π variations are required between mirror elements in which case the mirror subroutine is doing the wrong thing by removing such variations. This point is further discussed in Section II-D-1.

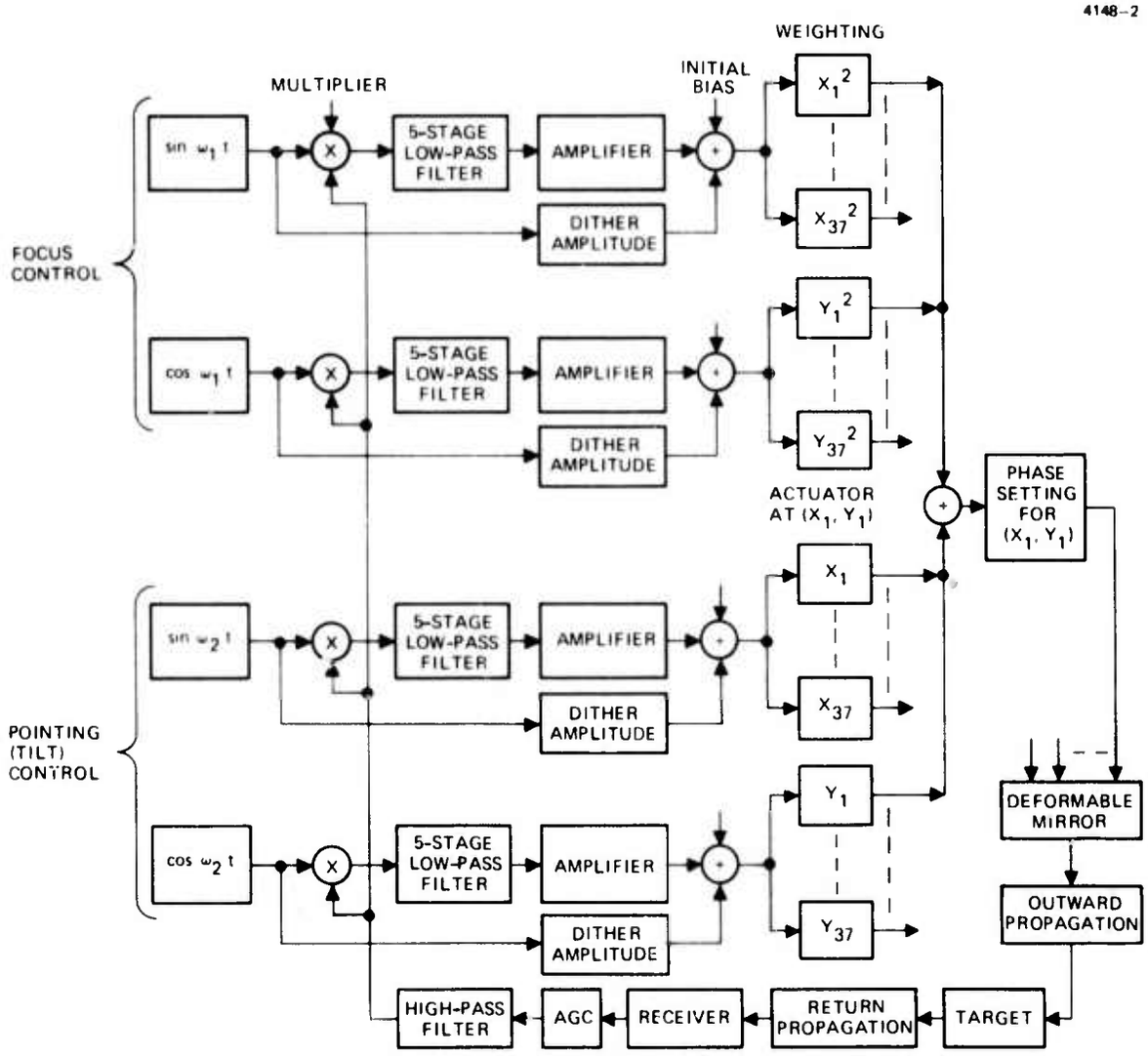

Fig. 8. Multidither servo simulation of two-channel focus and two-channel tilt control.

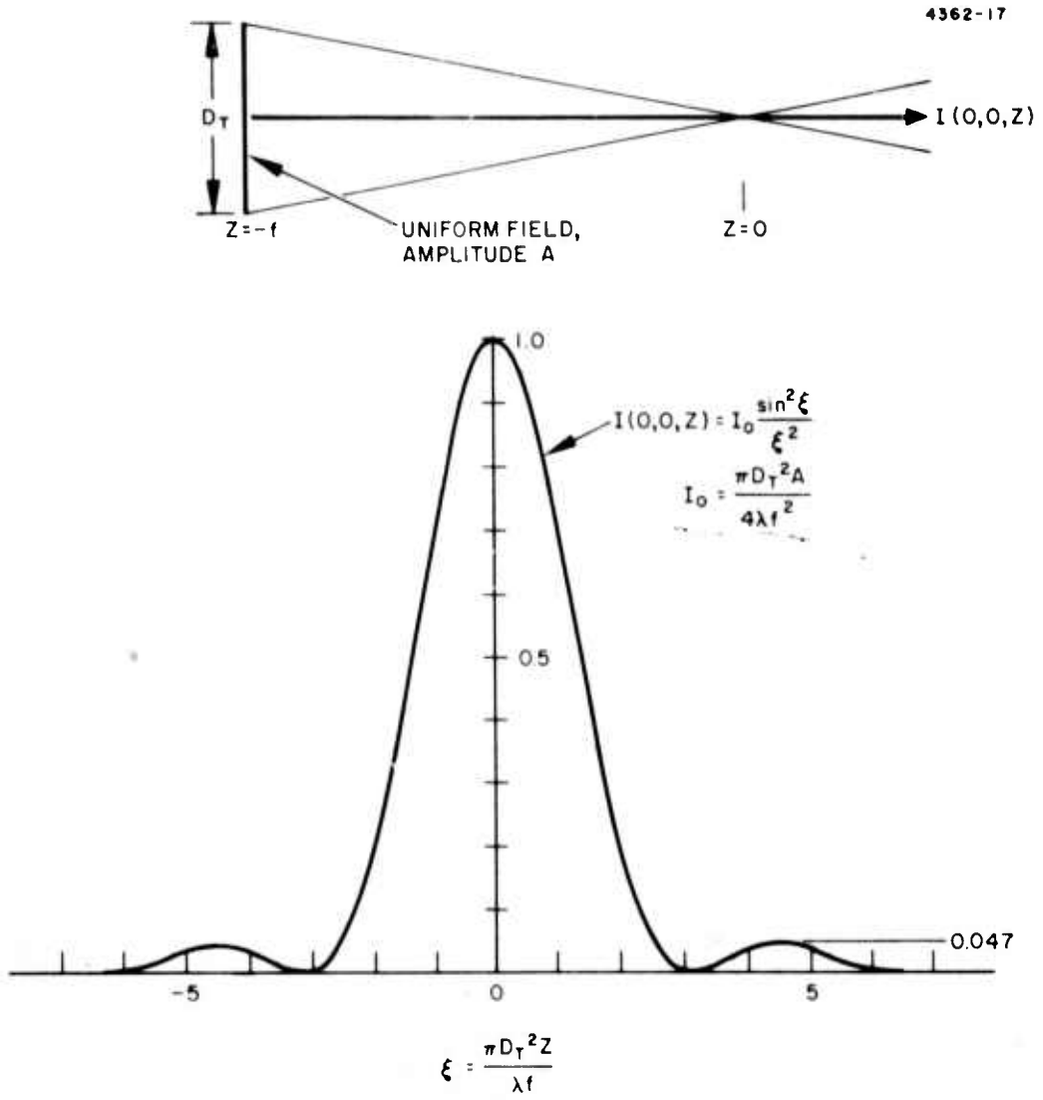

Fig. 9(a). Computer simulation of 2-axis BAT focus control using a 37-element deformable mirror. Behavior of on-axis intensity of a focused beam.

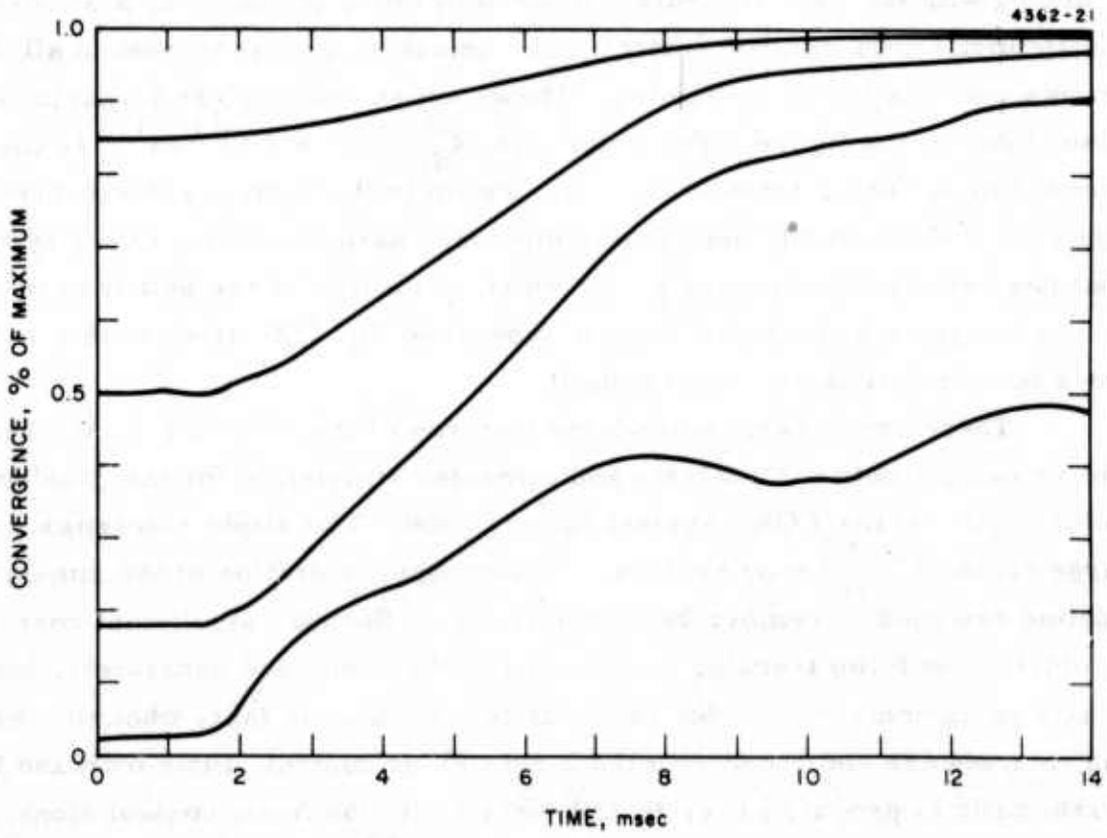

Fig 9(b) Computer simulation of 2-axis BAT focus control using a 37-element deformable mirror. Computer results showing two different stable convergence points which depend on the initial defocus.

We have made some computer runs to determine turbulence compensation using only the tracking and focus controls; no blooming compensation studies have been made because of the difficulties discussed in Section II-D. Figure 10 shows a summary of the compensation results achieved with the BAT controls compared to those produced by a 37-element multidither COAT control system. The deformable mirror used in all the simulation runs has 37 actuators. The assumed propagation scenario is also shown in the figure. For reference, $C_N^2 Z \gtrsim 21 \times 10^{-11}\ m^{1/3}$ is considered to be strong turbulence. Also shown in the figure is the theoretical limit for a 37-element, deformable mirror, phase-conjugate COAT system that has perfect phase-sensing, but which is limited by the ability of the mirror to provide the desired phase front (see Eq. (22) later in this report for a further discussion of this limit).

There are several noteworthy features of the data in Fig. 10. First, the agreement between analysis and computer simulation for the 37-element deformable mirror COAT system is very good. The slight discrepancy at large values of $C_N^2 Z$ may be caused by improper operation of the simulation routine designed to remove $2n\pi$ ambiguities.* Second, significant correction is obtained with the tracking or focus controls when used separately, but the 2-axis focus control provides the most correction. In fact, when the tracking controls are combined with the 2-axis focus control, little increase in strehl ratio is produced over that observed with the focus control alone. The significantly worse performance of a spherical** focus control above $C_N^2 Z = 40 \times 10^{-11}\ m^{1/3}$ is also interesting. Finally, not unexpectedly, a 37-channel multidither COAT system produces significantly more correction than the BAT controls alone; the BAT controls produce roughly a factor of 2 improvement in strehl ratio and the 37-channel COAT system can improve the strehl ratio another factor of 2. Experimental data that are in good agreement with these simulation results are presented in Section II-D-4.

---

*The tendency for some elements of a multidither system to converge within a multiple of 2π of the desired correction phase front when the initial errors are large.

**2-axis focus control with both axes driven by the same dither and correction signals.

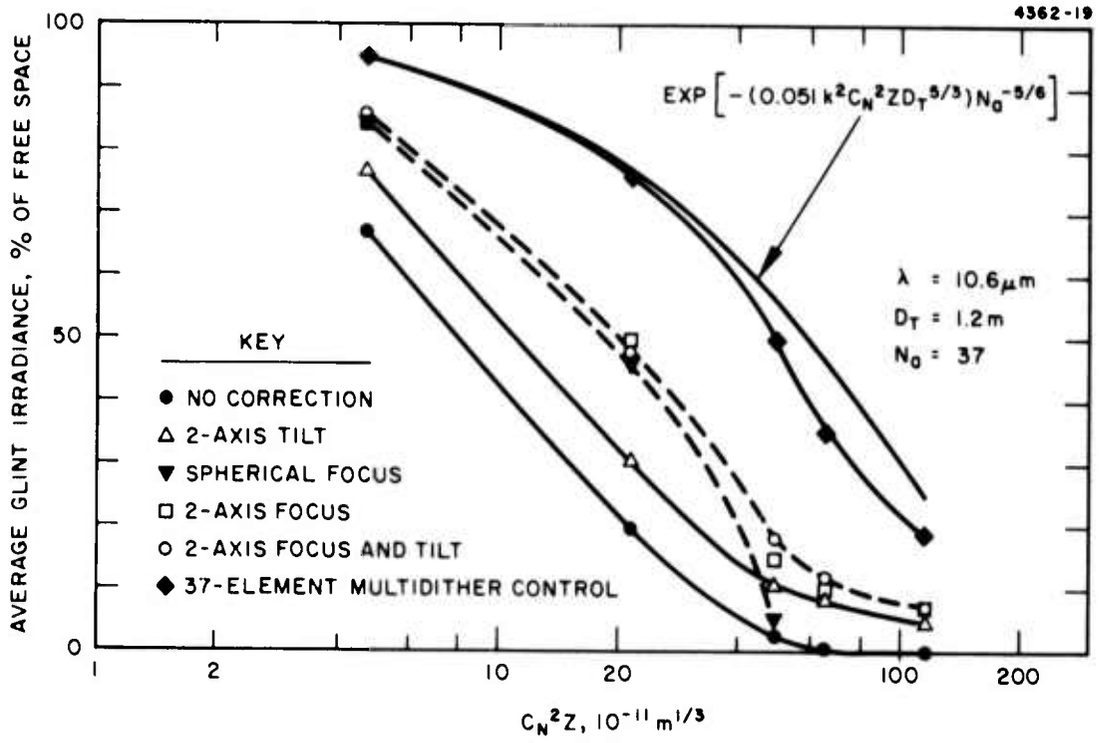

Fig. 10. Turbulence compensation produced by computer simulation using 37-element deformable mirror. Multidither COAT control is compared to BAT (tracking and focus control), focus control only (both spherical and 2-axis), and tracking control only.

B. COAT/Target-Signature Interactions

Contract Amendment No. 2 redirected some of the contract work to provide time and funds for some initial studies of the interaction of a multi-dither COAT servo system with backscatter from an extended, semi-diffuse target. Some of the results of these studies were presented at the 1975 Conference on Laser Engineering and Applications.[3] The interest in pursuing these studies was initially motivated by the work of Ogrodnik and Gurski.[4]

1. Problem Statement

The physical problem known as "speckle noise" can be stated briefly. When a coherent laser beam illuminates a target, some of the energy is scattered back in the direction of the transmitted beam. The backscattered radiation produces a random intensity pattern (a "speckle pattern") at a receiver, which is located close to the transmitter for cases of interest to us. When the appropriate conditions exist, any movement of this speckle pattern relative to the receiver will produce an amplitude modulation of the received signal. Since a multidither COAT system receiver senses amplitude modulations on the backscattered beam that are produced by dithering the transmitted beam phase, spurious amplitude modulations in the receiver may swamp the desired modulations and thus interfere with the system operation.

Doppler shifts produced by rapidly rotating targets may also produce false signals, but these spurious signals are expected to be less important than amplitude modulation effects for the target scenarios of interest. This is true because the most likely glint point on a rapidly rotating target is one normal to the beam incidence direction; this point will have nearly zero transverse doppler shift. Longitudinal doppler shifts are very narrow band and thus will have minimal effect on a multiple-channel COAT system.

Thus for COAT applications, it is important to determine three things about target-signature effects. First, what kind of modulations interfere with the proper operation of a multidither COAT system? The interesting parameters of the modulation are amplitude, frequency spectrum, and power spectral density. Second, what kind of receiver modulations are produced by

backscatter from real targets in expected operational scenarios? That is, what scenarios will produce the modulations that can affect the COAT system? Third, can a multidither COAT system be designed that is insensitive to speckle-induced receiver modulation and if so, what are the critical design parameters? An expected follow-on contract to the current contract is designed to produce definitive answers to all these questions. Some preliminary studies of the magnitude of the effects are being pursued on the present contract, however.

2. Experimental Results

For a first experiment, we chose the simple extended moving target shown in Fig. 11(a). The target is a cylindrical scotchlite strip that could be rotated at different rates. The target is larger than the COAT-formed array pattern in both dimensions (parallel to and perpendicular to the rotation axis), but exceeds the element pattern diameter only in one dimension. The curvature of the scotchlite provides a localized highlight on which the COAT system can lock. The laboratory experimental arrangement used is shown in Fig. 11(b). No turbulence or blooming was introduced in the paths and the BAT controls were not used. The receiver/transmitter aperture ratio was chosen to be 0.66.

The experiment consisted of observing the peak target irradiance and the COAT receiver signal frequency spectrum when the target was stationary and moving. Figure 12 shows the observed receiver power spectra for several cases. The figures show a spectrum analyzer output when the input is the COAT photomultiplier signal. The spectrum analyzer bandwidth was 10 Hz in Figs. 12(a) and (b), and 200 Hz in (c) and (d). Each photograph consists of five 2-minute scans over a 0 to 50 kHz range. Figures 12(a) and (c) are the observed spectrum when the target is stationary and Figs. 12(b) and (d) are the spectrum when the target rotates. The target rotation speed was chosen to give the largest observed change in the spectrum over the dither band. For the stationary targets, the noise level is low and the dither signals are clearly evident above the noise. When the target is moving, the noise level increases significantly and most of the dither signals are no longer evident. The peak target irradiance was the same, however, whether the

(a)

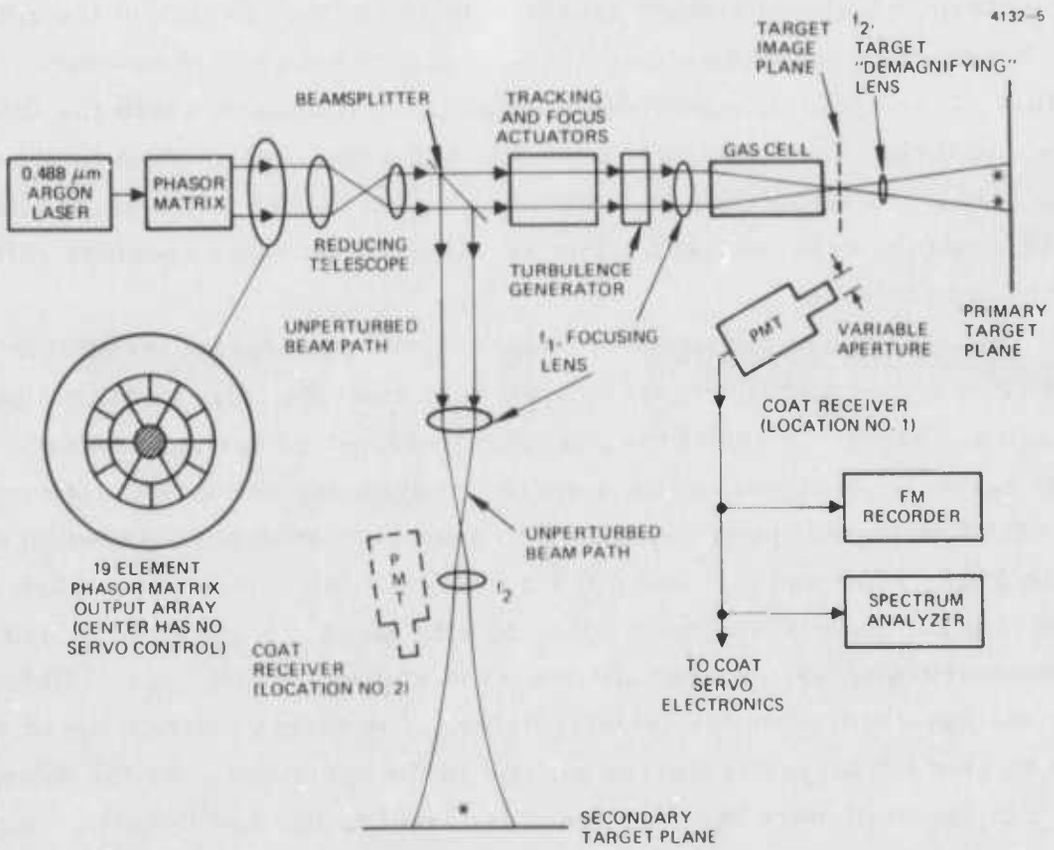

(b)

Fig. 11. Experimental apparatus for COAT/target studies. (a) Rotating scotchlite cylinder used for target. (b) Schematic of optical setup.

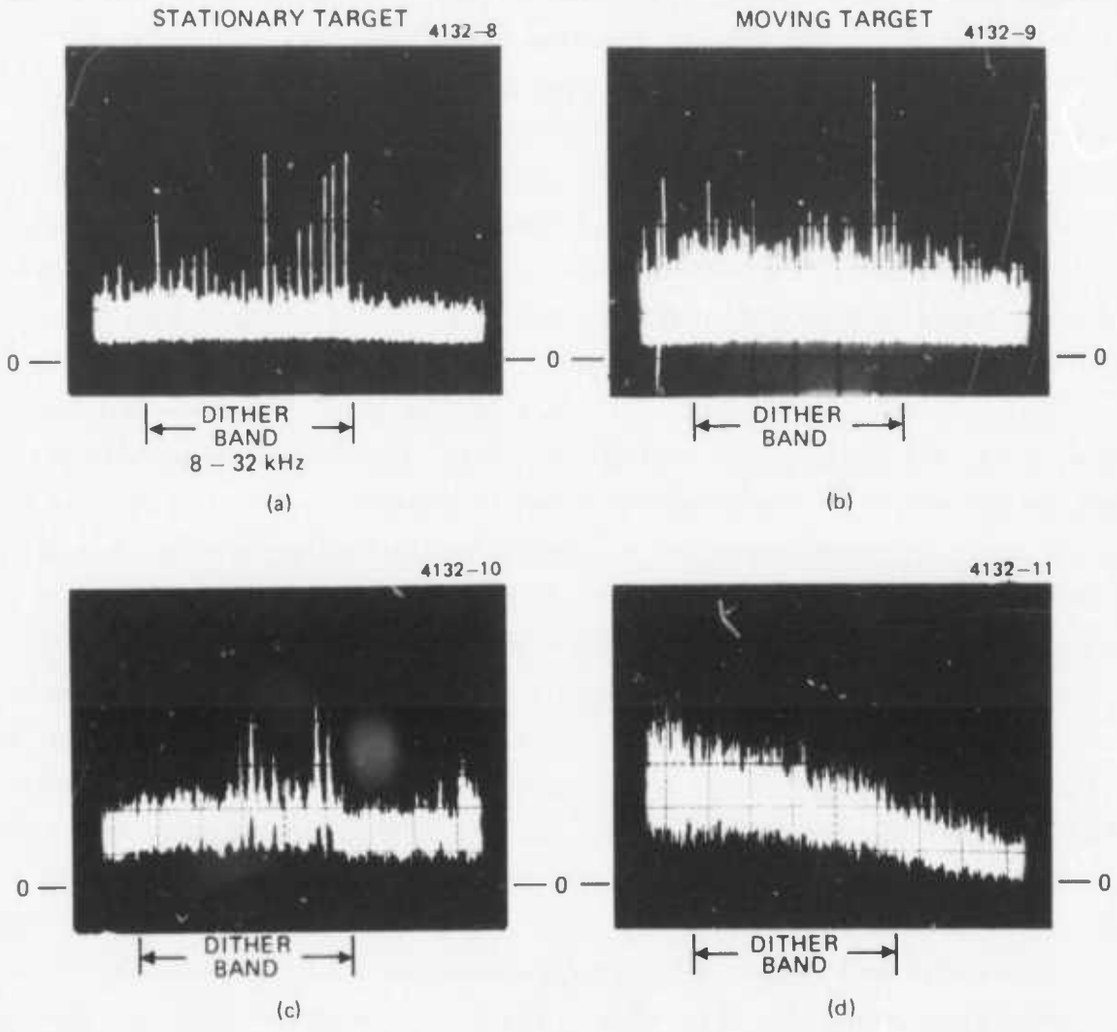

Fig. 12. COAT receiver signal power spectra for cylindrical strip, scotchlite target. (a) and (c) stationary target, (b) and (d) rotating target. The spectrum analyzer bandwidth is 10 Hz in (a) and (b) and is 200 Hz in (c) and (d).

target was stationary or moving. For this simple target, if the COAT system could converge on the target when it was stationary, the system could converge equally well when the target was moving. For every target and target motion rate that we have tried to date, this same observation has been made: no noticeable effects when the target moves.

The observation of no effect on the COAT system performance is contrary to a statement made in the third management report. The very earliest experiments did seem to show some effect. What we found, however, was that very large extraneous dither signals were being introduced into the COAT receiver by ground loops, not by target speckle effects. Since the ground loops have been eliminated, we have not been able to find a target which "confused" the COAT system solely because of its motion.

Since we have seen no deleterious COAT-system/target-modulation effects, a natural question is: "What kind of spurious signals can reduce the system performance?" We thus undertook an experiment whose goal was to generate large amplitude spurious amplitude-modulated signals capable of overloading the dither servo channels. In this experiment, the target was a single glint and a large receiver aperture was used. Spurious amplitude modulations were artificially introduced into the COAT system by putting an acousto-optic modulator (AOM) in the optical beam path, as shown in Fig. 13. The AOM amplitude modulates the transmitted beam at a frequency set by the voltage-controlled-oscillator (VCO), shown in Fig. 13. Figure 14 shows the modulated light incident on the target glint when the oscillator was not swept in frequency. Modulation depths of 64% were observed over the dither frequency band (8 to 32 kHz) with a triangular-wave drive to the VCO.

Manually tuning the VCO through the dither passband sequentially overloaded the feedback loop at each dither frequency and caused a 10% reduction in peak target irradiance (a loss of proper phasing in 1 of the 18 COAT channels). Spectrum analyzer measurements indicated that the spurious signal level of 100 mV generated in this manner was much larger than the 3 mV dither amplitudes. This initial result establishes the fact that external modulation applied to the COAT beam could overload the control circuitry in any single channel and cause the loss of that channel in forming the converged beam.

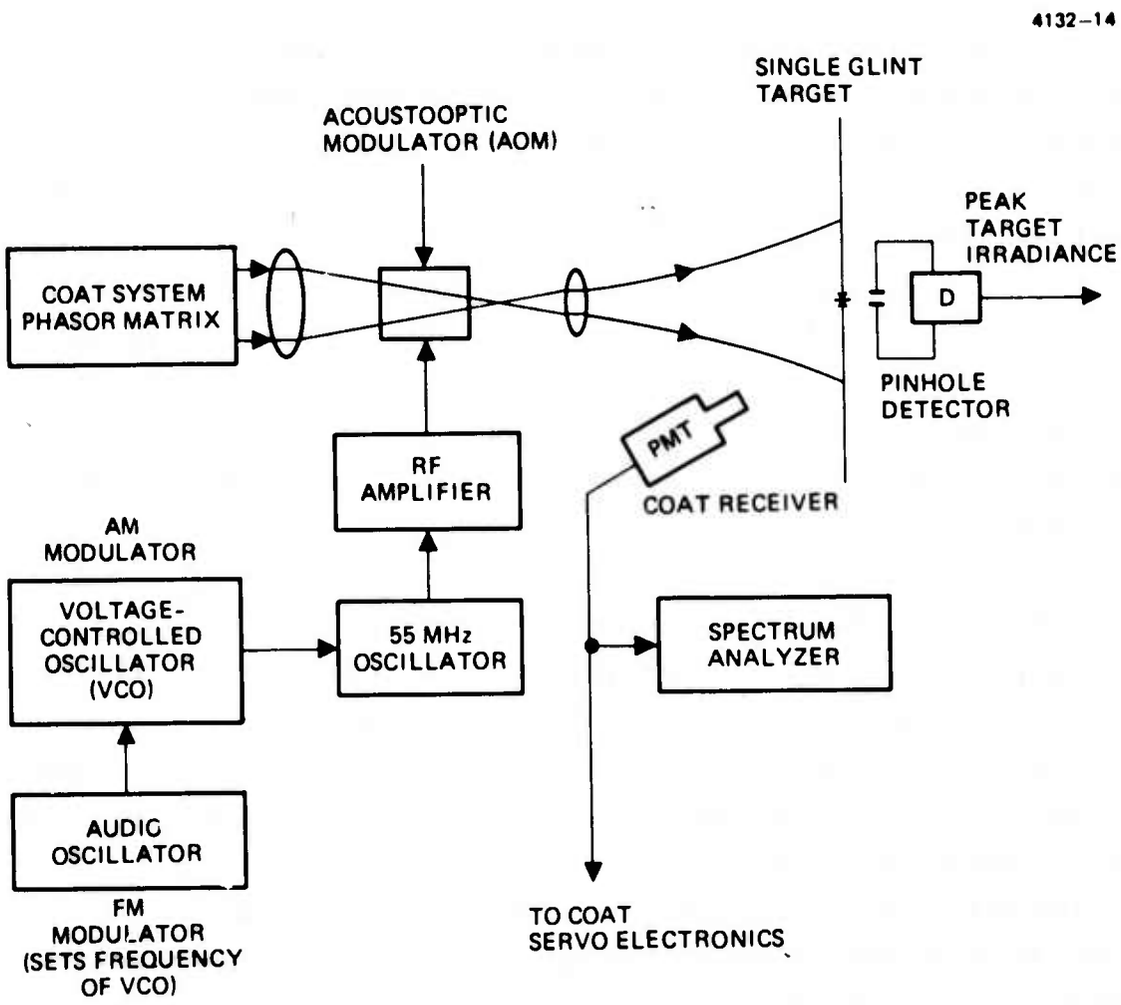

Fig. 13. Experimental setup to determine effect of spurious amplitude modulations in a COAT receiver.

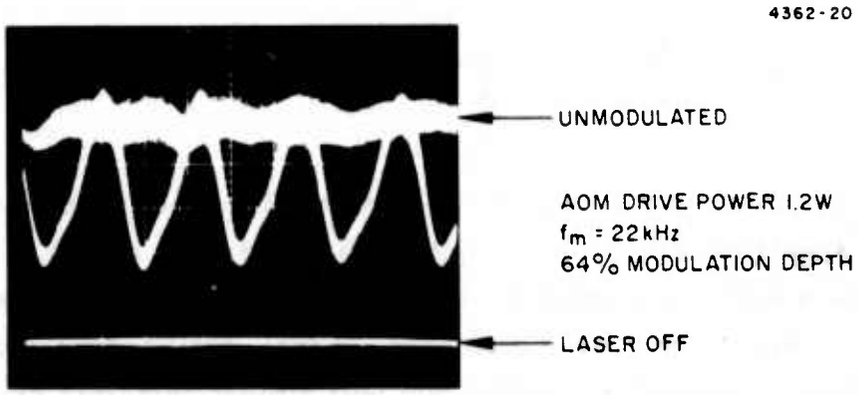

Fig. 14. Light intensity incident on target with acousto-optic modulator (AOM) in the optical path.

To roughly simulate the effect of worst-case broadband speckle modulations, the VCO was swept over a selectable bandwidth with sweep periods of 1 msec and 0.5 msec (shorter time than the COAT system convergence time of 1.5 to 2.0 msec). During this series of tests, the COAT receiver frequency spectrum was recorded and the power level in the converged beam was measured with the sweep voltage turned on and off. The resulting spectra for six different sweep bandwidths and a 1 msec sweep period (0.5 msec across the sweep bandwidth) are shown in Fig. 15. The center frequency, f_o, was selected for maximum effect on the COAT system. The sweep bandwidths in Fig. 15 range from 1 kHz to 30 kHz ($f = f_o \pm BW/2$), but the ratio of the peak target irradiance with the spurious modulation to that without it (P_{mod}/P_o) is nearly constant. A value of $P_{mod}/P_o = 0.69 = (15/18)^2$ corresponds to a loss of proper phasing in three channels on the average and $(14/18)^2 = 0.60$ corresponds to a loss of 4 channels. Similar results are obtained when the sweep period is reduced to 0.5 nsec. A graph of the number of active elements lost versus modulation bandwidth is shown in Fig. 16(a) and the corresponding loss of converged beam power loss versus modulation bandwidth is shown in Fig. 16(b).

The power spectrum of the triangular-wave swept modulation used here consists of a sum of all the harmonics of the sweep frequency spaced about the center frequency:

$$P_m = \sum_{n=-\infty}^{\infty} a_n \exp\left[i2\pi \left(f_o - n f_{sweep}\right)\right] \qquad (5)$$

where the a_n are determined in part by the sweep bandwidth. Although this type of power spectrum will probably <u>not</u> be characteristic of any target-induced speckle spectrum, it does have several properties which a speckle-induced receiver spectrum should also have. First, the bandwidth of the extraneous receiver signals is limited, but will almost certainly exceed 35 kHz in cases of most interest.[4] Second, the product of peak power

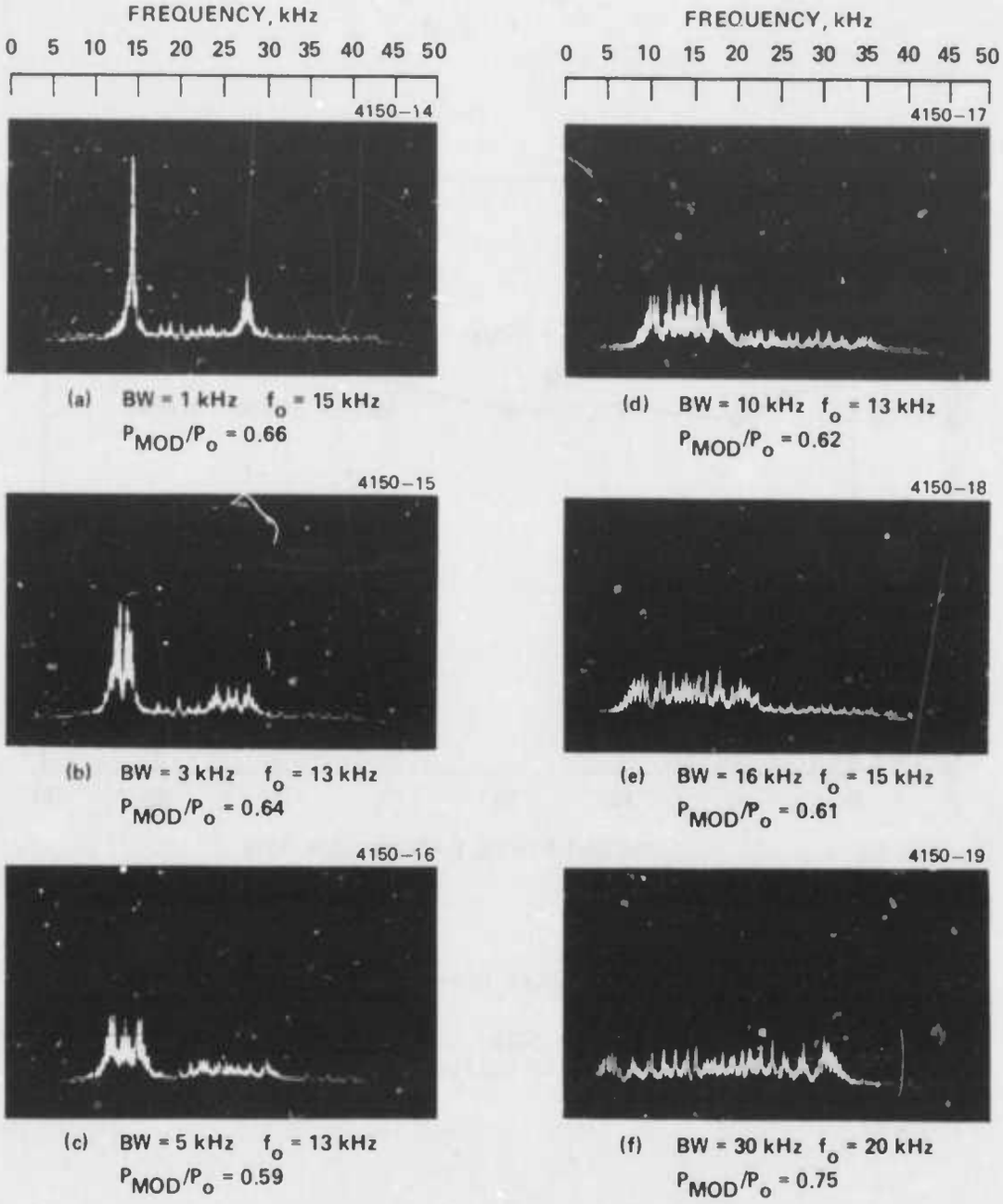

Fig. 15. COAT receiver power spectra for different sweep bandwidths for the AOM drive (see Fig. 13). The sweep period is 1 msec.

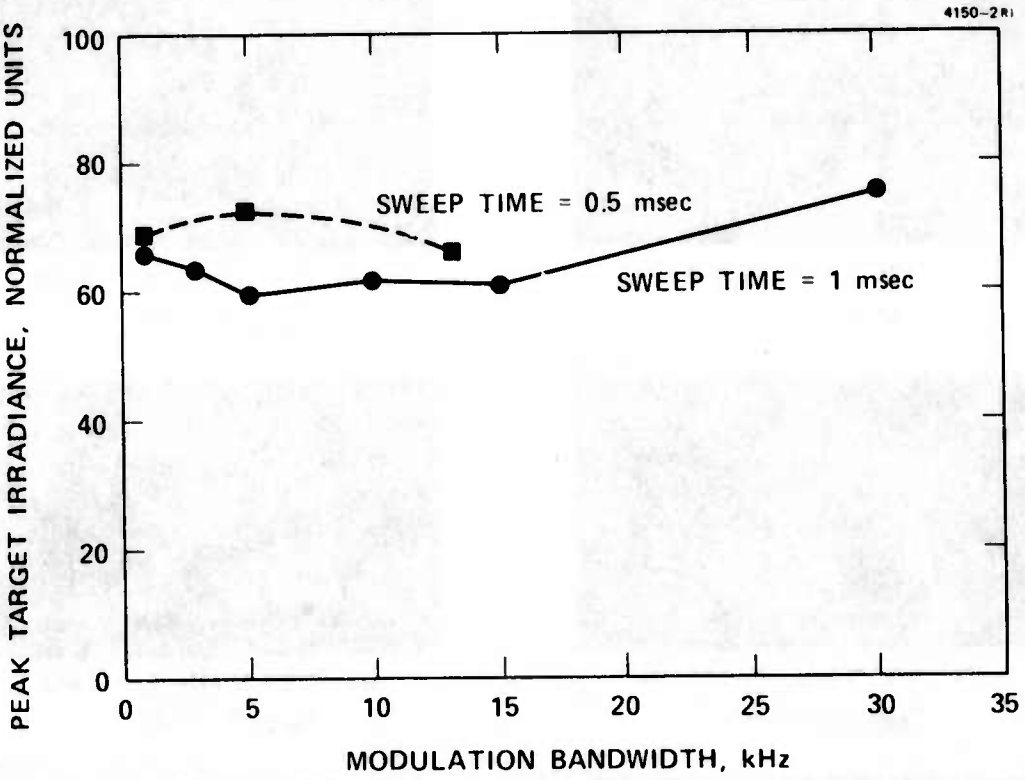

(a) Observed peak target irradiance.

Fig. 16. Effect of acousto optic modulation on DARPA/RADC COAT system as a function of total modulation bandwidth.

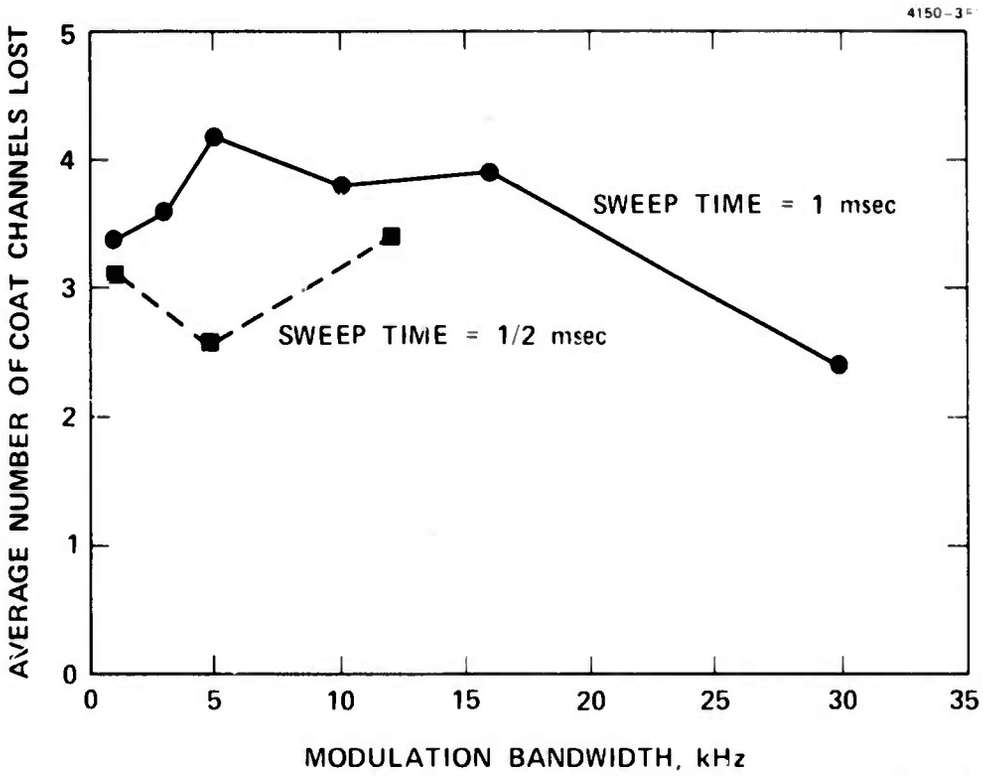

(b) Average number of inoperatige COAT channels corresponding to irradiance loss in (a).

Fig. 16. Effect of acousto optic modulation on DARPA/RADC COAT system as a function of total modulation bandwidth.

spectral amplitude and bandwidth is constant. The experimental AOM data obey such a relationship as demonstrated in Fig. 17. What this means is that the receiver can see a 100% average modulation-depth signal at only a single frequency; as the modulation bandwidth increases, the average receiver voltage modulation depth (not the instantaneous depth or amplitude) goes down as th reciprocal of the square root of the bandwidth.

Determination of the actual spectrum of a real speckle-induced receiver signal is beyond the scope of this contract. As a worst case, however, consider a spectrum of equal amplitude sinusoidal frequencies, spaced by 100 Hz over a 35 kHz bandwidth,* which is close to a worst-case situation. Since there are 350 frequencies, the average receiver voltage modulation depth for any one must be $(350)^{-1/2} \approx 0.042$, or 4.2% to maintain a constant power-bandwidth product. This assumes a 100% speckle modulation depth, which will occur only for purely diffuse targets. If we take a 50% modulation depth since realistic targets will probably have some specular returns, the average modulation depth drops to 2.1%. This value is below the 5.6% peak receiver modulation produced by a multidither system operating with a $\pm 20^{\circ}$ dither modulation.

A further consideration that we have not taken into account is that the spectral components of speckle-induced receiver noise will have randomly varying phases with respect to the dither modulation. The servo synchronous detectors will thus further discriminate against this type of noise. We expect to have an analytical demonstration of the magnitude of this discrimination sometime in the near future.

These brief studies seem to indicate that target-signature effects are not going to be as severe as was thought earlier. More realistic targets and motions need to be studied, however, and other effects such as more servo channels or receiver signal-to-shot noise need to be investigated. The presence of turbulence or blooming may also have some effect.

*A more realistic speckle-induced spectrum might be a uniform triangular or Gaussian distribution with a 50 kHz bandwidth.

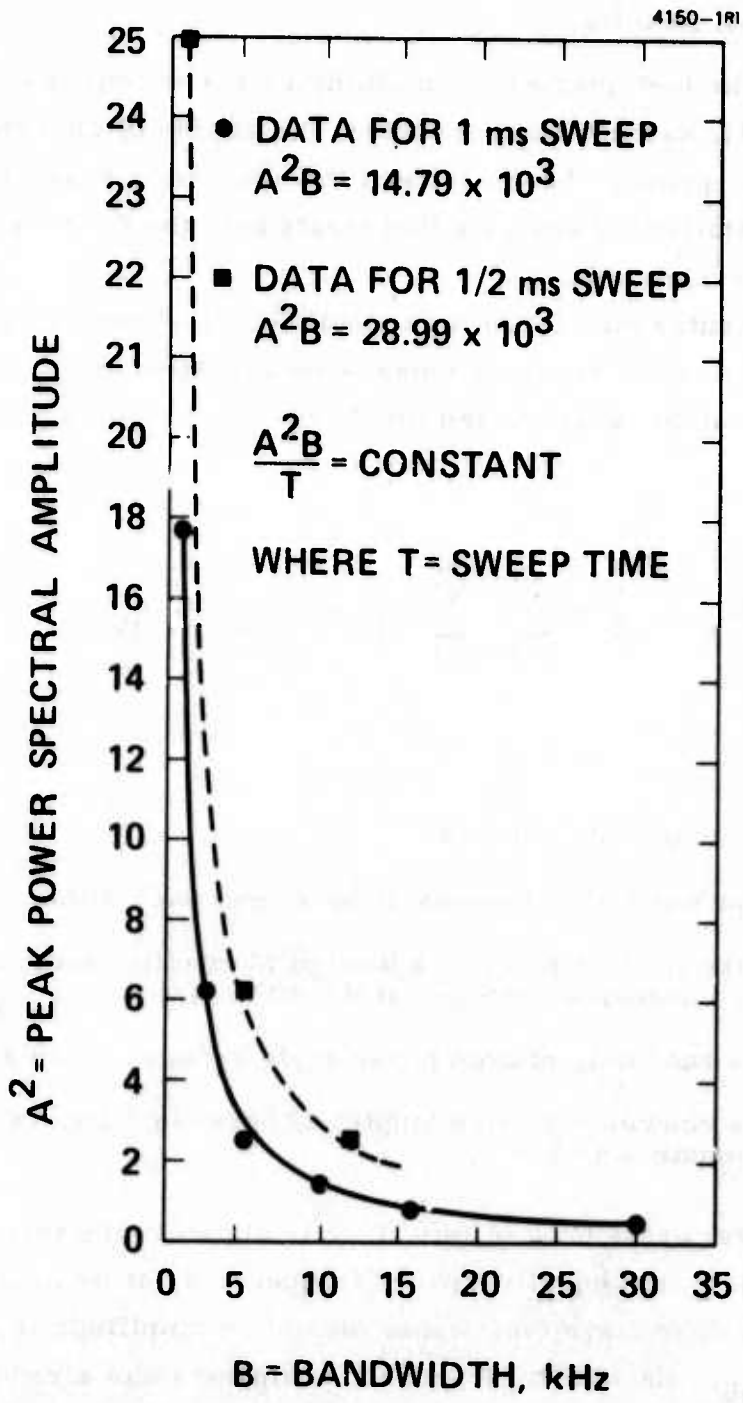

Fig. 17. Peak power spectral amplitude versus bandwidth for the AOM experiment.

3. Analytical Results

During the last quarter the multidither servo computer simulation developed at HRL was modified to include the effects of speckle modulation on system convergence. The results of the simulation have also been compared to a statistical analysis that treats both the COAT system and a model of the speckle noise.

The computer simulation was modified, as shown in Fig. 18, to include a multiplicative receiver noise – the speckle-induced noise. The amplitude modulation noise chosen for these initial studies has the following form:

$$M_s \equiv \frac{1}{2} + \sum_{k=1}^{N} \sum_{j=1}^{M} a_{jk} \sin (\omega_{jk} t + \phi_{jk}) \quad , \qquad (6)$$

where:

$N \equiv$ number of channels

$M \equiv$ number of erroneous signals near each dither frequency

$\omega_{jk} \equiv$ the jth frequency in a band of M equally incremented frequencies centered at the dither frequency ω_k

$\phi_{jk} \equiv$ a randomly chosen phase angle between 0 and 2π

$a_{jk} \equiv$ a randomly chosen amplitude between 0 and an adjustable maximum, a_{max}.

A typical spectral breakdown of this noise is shown in the inset to Fig. 19(c). There are 21 discrete, equally-spaced frequencies, at or near each dither frequency of the COAT system, whose maximum amplitude is set by the parameter a_{max}. Each noise frequency component has a randomly chosen amplitude and phase. This signal multiplies the usual COAT receiver signal.

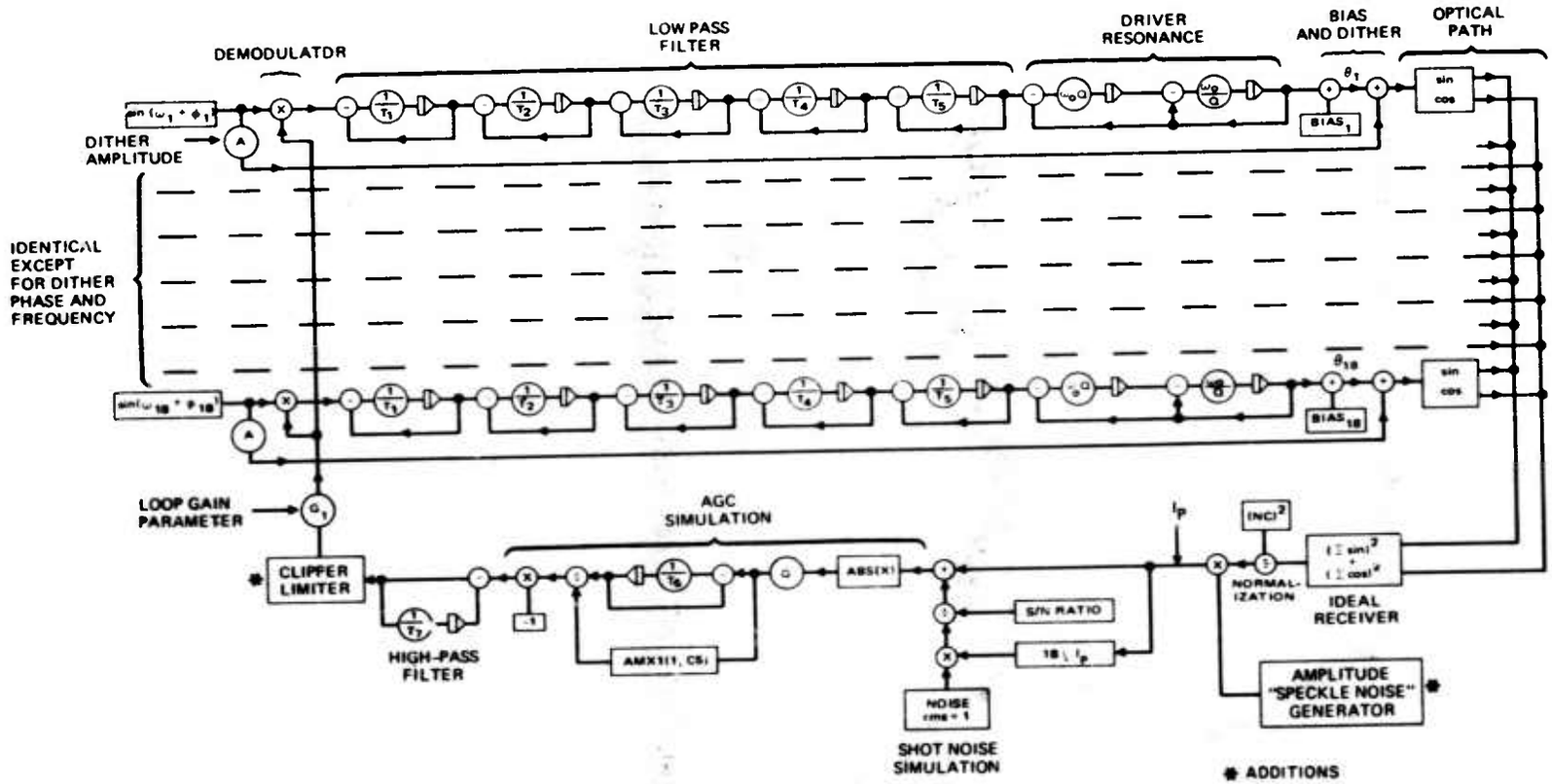

Fig. 18. COAT servo simulation showing addition of "speckle" noise generator.

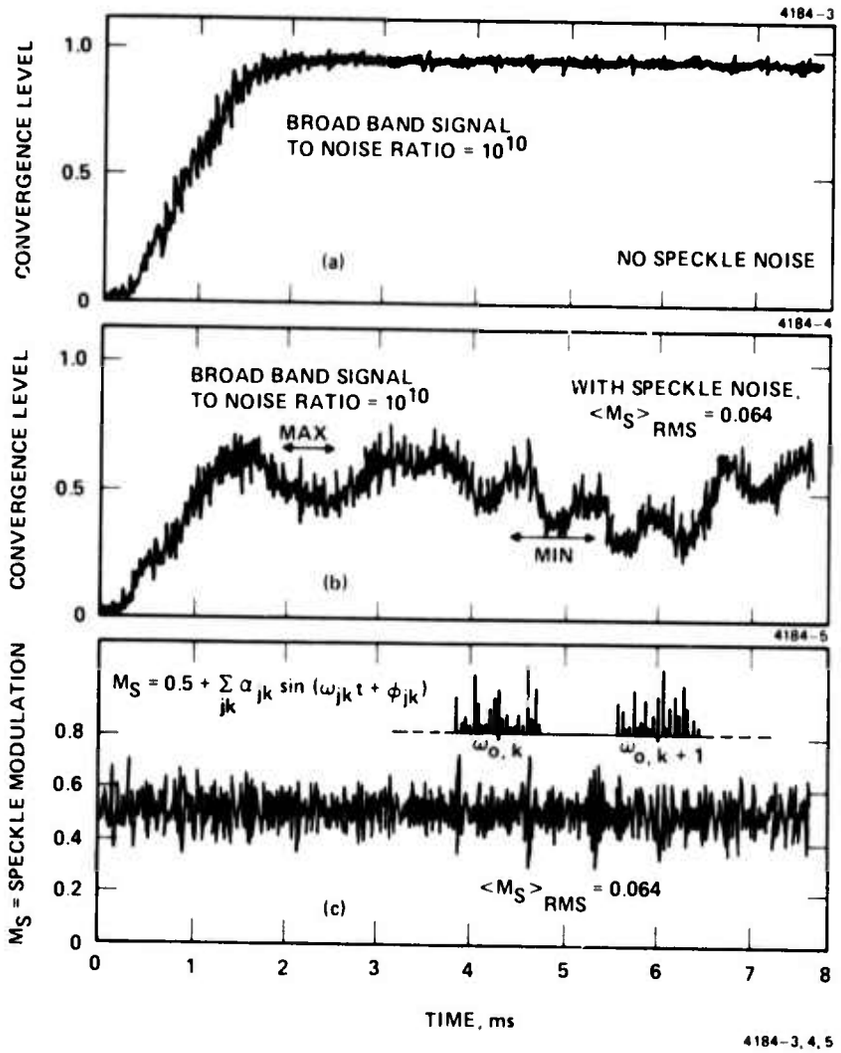

Fig. 19. COAT computer simulation time histories. (a) Broadband shot noise signal-to-noise ratio = $(S/N_{shot} = 10^{10}$ and $a_{max} = 0$ (no speckle noise). (b) $a_{max} = 0.008$ corresponding to $\langle M_s \rangle = 0.064$. (c) Speckle noise modulation used to produce (b).

For the simulation studies performed to date, the 21 noise frequencies are spaced ±83 Hz around each dither frequency. This is a rather arbitrary choice, but it does insure that all spurious modulation is well within the 400 Hz servo bandwidth. An amplitude limitation was also included to keep the return signal from exceeding an absolute value of unity just before entering the loop gain amplifier (noted as G_1 in Fig. 18). This modification, which avoids instabilities resulting from the automatic gain control mechanization, is used in the lab model of the COAT array. Simulations were run at three values of broad-band signal-to-noise ratio (receiver shot noise): 10^{10}, 40, and 20. When $(S/N)_{shot} = 10^{10}$ and $a_{max} = 0$ (no speckle noise), the simulation produces a time history of the power on the target glint as shown in Fig. 19(a). When the speckle noise modulation shown in Fig. 19(c) is present ($a_{max} = 0.008$ and $\langle M_s \rangle = 0.064$ - See Eq. (6)), the time history in Fig. 19(b) results. Notice that although the rms value of M_s is only 0.064 (around $M_s = 0.50$), the maximum peak-to-peak value is about 0.4.

The behavior shown in Fig. 19(b) for $a_{max} \neq 0$ is typical. In general, the speckle noise has two effects: (1) the maximum percent convergence level is lowered; and (2) a random oscillation of the intensity occurs between the new maximum convergence level and a minimum level. This oscillation is much slower than the dither oscillations and its magnitude varies with convergence level. Figure 20 shows a plot of the maxima and minima recorded during these simulations as a function of a_{max}. The open loop gain, G_1, was the same for each case. At high average convergence levels (low values of a_{max}), the random oscillations have much smaller magnitudes than at the low convergence levels (high values of a_{max}).

In order to understand the behavior of the multidither COAT system with multiplicative speckle noise, we have begun a statistical analysis of such a COAT system which includes the speckle noise. The analysis is not yet complete, but it does provide some understanding of the COAT system operation.

The object of the analysis is to explain, and if possible, to predict the behavior observed in the computer simulations. Note that the voltage generated at the photomultiplier is proportional to the intensity of the radiation incident on it. The servo error information contained in this signal consists of modulations at the dither frequencies, ω_n. If the reflected

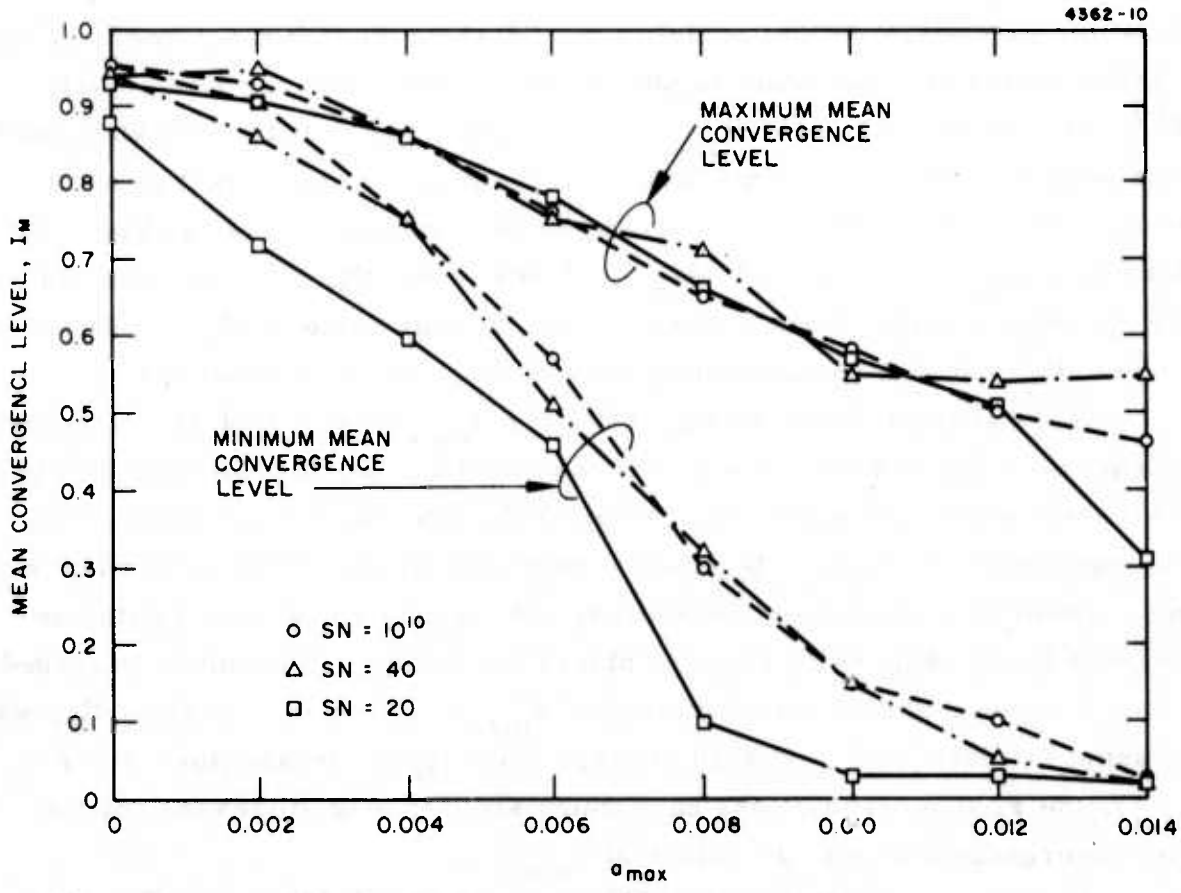

Fig. 20. COAT convergence levels as a function of speckle noise amplitude as observed by computer simulation.

intensity is further modulated by the speckle noise function M_s, false error information is generated in the servo loop. The voltage at the dither frequencies will then consist primarily of the sum of the correct error information plus the false error signal. Other sources of noise at these frequencies are ignored in this analysis.

As we have just stated, the total error signal, S_e, is just the sum of S_D, the correct dither error signal, and S_s, the false error signal due to speckle (both in volts). The strength of the dither signal depends on the convergence level while the strength of the speckle signal depends on both the convergence level and the parameter a_{max}. Based on preliminary calculations, we hypothesize that the time-averaged convergence level maintained by a COAT system with a speckle modulation M_s, corresponds to a fixed ratio of the average dither signal power to the average speckle modulation signal power. With this hypothesis in mind, we will calculate the expectation values of these average powers as a function of the parameters a_{max} and the mean convergence level I_M, which will be defined shortly. Expressions will be derived which will enable us to relate the three parameters a_{max}, I_M, and the power ratio $\rho = S_D^2/S_S^2$.. This will allow us to calculate I_M as a function of a_{max} at fixed values of ρ. If the above hypothesis is correct, then these curves should predict the same kind of behavior as the simulation data in Fig. 20.

Consider the electric field of N separate waves having the same amplitude and wavelength incident on a given point. Assume the polarization of each wave is adjusted so that they are all plane polarized parallel to each other. Then the total field, E_T, is

$$E_T(t) = \sum_{n=1}^{N} E_o \, e^{i\Gamma_n(t)} \tag{7}$$

where E_o is the magnitude of each wave (assumed equal for each wave), and $\Gamma_n(t)$ is the time-varying phase of the n^{th} wave at the target glint.

The radiant intensity is equal to the absolute square of the electric field. Consequently, a radiant intensity normalized to unity when all $\Gamma_n = 0$, may be written as:

$$I_T = \frac{1}{N^2} \sum_{n=1}^{N} \sum_{m=1}^{N} E_o^2 \exp i[\Gamma_n(t) - \Gamma_m(t)] \quad . \tag{8}$$

In the COAT multidither array the N phase angles are physically dithered at different frequencies. For such an array the phase in the n^{th} channel $\Gamma_n(t) = \beta_n(t) + \psi \sin \omega_n t$. In this situation $\beta_n(t)$ represents a mean phase angle and ψ is the amplitude of the small dither deviation from the mean (typically $\psi < \pi/6$ radians). Substituting $\Gamma_n(t) = \beta_n(t) + \psi \sin \omega_n t$ into eq. (8) and expanding the result in Bessel functions gives

$$I_T = \frac{1}{N} + \frac{1}{N^2} \sum_{\substack{n=1 \\ n \neq m}}^{N} \sum_{m=1}^{N} e^{i(\beta_n - \beta_m)} \left[\sum_{k=-\infty}^{\infty} J_k(\psi)\, e^{ik\omega_n t} \right.$$

$$\left. \sum_{\ell=-\infty}^{\infty} J_\ell(-\psi)\, e^{i\ell\omega_m t} \right] \quad . \tag{9a}$$

Since we are only interested in the dither error signal and the convergence level, we need to consider only the first two terms in the Bessel expansions:

$$I_T = \frac{1}{N} + \frac{1}{N^2} \sum_{\substack{n=1 \\ n \neq m}}^{N} \sum_{m=1}^{N} \left\{ \cos(\beta_n - \beta_m) \left[J_o^2(\psi) + \ldots \right] \right.$$

$$+ \sin(\beta_n - \beta_m) \left[-2J_1(\psi)\, J_o(\psi) \left(\frac{e^{i\omega_n t} - e^{-i\omega_n t}}{2i} \right) \right. \tag{9b}$$

$$\left. \left. + 2J_1(\psi)\, J_o(\psi) \left(\frac{e^{i\omega_m t} - e^{-i\omega_m t}}{2i} \right) + \ldots \right] \right\} \quad .$$

Thus we can separate out I_M, the mean convergence level, and I_D, the modulations at the dither frequencies.

$$I_M \equiv \frac{1}{N} + \frac{J_o^2(\psi)}{N^2} \sum_{\substack{n=1 \\ n\neq m}}^{N} \sum_{m=1}^{N} \cos(\beta_n - \beta_m) \tag{10}$$

$$I_D \equiv - \frac{4J_o(\psi)\, J_1(\psi)}{N^2} \sum_{\substack{n=1 \\ n\neq m}}^{N} \sum_{m=1}^{N} \sin(\beta_n - \beta_m) \sin \omega_n t \, . \tag{11}$$

We can now express the intensity on the glint as

$$I_T = (I_M + I_D + I_N) \cong I_M + I_D \, , \tag{12}$$

where I_N is the sum of all modulations in eq. (9) that are not included in I_D (i.e., modulations at harmonics plus sum and differences of the dither frequencies). These can be considered as noise since they are not used in the servo system to generate error information and since they are higher order terms in the variable ψ.

In the simulations, the total intensity incident on the photomultiplier is given by the product $M_s I_T$. Combining eqs. (6) and (12) gives

$$M_S I_T \cong \frac{1}{2} I_M + \frac{1}{2} I_D + I_M \sum_{k=1}^{N} \sum_{j=1}^{M} a_{jk} \sin(\omega_{jk} t + \phi_{jk})$$

$$+ I_D \sum_{k=1}^{N} \sum_{j=1}^{M} a_{jk} \sin(\omega_{jk} t + \phi_{jk}) \, . \tag{13}$$

The second and third terms in eq. (13) are the ones we are interested in. The second term contains the correct dither information, while the third contains the false dither signal from the speckle noise. The first term is a dc term representing the mean intensity at the receiver and thus is not important to our discussions. The last term consists of intensity modulations at or near harmonics and sums and differences of dither

frequencies. This term can be neglected for two reasons. First, most of the modulations will be outside the dither band and will therefore be filtered out by the low-pass filter in the servo electronics. Second, since it is proportional to I_D, it is an order of magnitude smaller than the third term, which is proportional to I_M.

The voltages S_D and S_S are thus proportional to the second and third terms respectively. Letting K be the photomultiplier proportionality constant, we have

$$S_D = \frac{1}{2} K I_D \tag{14}$$

and

$$S_S = KI_M \sum_{k=1}^{N} \sum_{j=1}^{M} a_{jk} \sin(\omega_{jk} t + \phi_{jk}) \quad . \tag{15}$$

When the COAT system reaches a steady state convergence level (such as that shown in Fig. 19(b) for example), we can calculate the average dither signal power, P_D, and the average speckle signal power, P_S, normalized to unit resistance by using eqs. (14) and (15). The results are

$$P_D = \frac{K^2}{8} \left(\frac{4J_o(\psi)\, J_1(\psi)}{N^2} \right)^2 \sum_{n=1}^{N} \left[\sum_{\substack{m=1 \\ m \neq n}}^{N} \sin(\beta_n - \beta_m) \right]^2 \tag{16}$$

and

$$P_S = \frac{1}{2} K^2 I_M^2 \sum_{k=1}^{N} \sum_{j=1}^{M} a_{jk}^2 \quad . \tag{17}$$

We now want to calculate the power ratio as a function of convergence level or, in other words, as a function of I_M. In order to do this, we need a statistical model of an N-channel COAT array at a steady state convergence level. This will allow us to calculate expectation values of P_D, P_S,

I_M and any other desirable quantities as a function of a statistical parameter α, which characterizes the convergence level.

In order to define the parameter α, we first recognize that the phase angles β_n are distributed over a limited overall angular spread. We define the magnitude of this spread as α. This can best be understood in terms of a phasor diagram. In Fig. 21, for example, we show the N phases as more or less uniformly distributed over an angle α. As α approaches zero, the laser array will converge (i.e., $I_T \rightarrow 1$ and thus $I_M \rightarrow 1$). Conversely, as α approaches 2π, the array approaches a convergence level of zero. The range of all possible relative phase differences, $\beta_m - \beta_n$, between any two channels, at a specified convergence level, is thus 0 to α. The quantity α therefore characterizes the convergence level, recognizing, of course, that this is true only in a statistical sense. We now make the rather arbitrary assumption that for a given convergence level, the N phases β_n are uniformly distributed between α_o and $\alpha_o + \alpha$ as shown in Fig. 21. We do not expect our results to depend strongly on the assumed distribution, and a uniform distribution simplifies the computations. The probability density that a given $\beta_n = \beta$ is just $P(\beta) = \alpha^{-1}$ over this range and zero everywhere else. The probabiliy density $P(\Delta\beta)$, for an arbitrary $\beta_m - \beta_n = \Delta\beta$, is the autocorrelation function of $P(\beta)$, given by

$$P(\Delta\beta) = \frac{1}{\alpha} - \frac{|\Delta\beta|}{\alpha^2} \quad . \tag{18}$$

This expression holds in the region $-\alpha < \Delta\beta < \alpha$. Outside that region $P(\Delta\beta) \equiv 0$.

Knowing the probability distribution allows us to calculate various expectation values. Consider, for example, the expectation value of I_M. Using the definition of I_M in eq. (10) gives

$$\langle I_M \rangle = \frac{1}{N} + \frac{J_o^2(\psi)}{N^2} \sum_{\substack{n=1 \\ n \neq m}}^{N} \sum_{m=1}^{N} \langle \cos(\beta_n - \beta_m) \rangle \quad . \tag{19}$$

Using eq. (18), it is easy to show that

$$\langle \cos(\beta_n - \beta_m) \rangle = \int_{-\infty}^{\infty} P(\Delta\beta) \cos(\Delta\beta) d(\Delta\beta) = \frac{2}{a^2} (1 - \cos a) \quad . \tag{20}$$

Thus we have

$$\langle I_M \rangle = \frac{1}{N} + J_o^2(\psi) \left(1 - \frac{1}{N}\right) \frac{2}{a^2} (1 - \cos a) \quad . \tag{21}$$

Figure 22 shows a plot of $\langle I_M \rangle$, versus a for an 18-element array, and a peak dither amplitude of $\psi = 0.349$ radians (20^o).

During the next quarter we will use this analysis to calculate expectation values of P_D, P_S and their ratio, ρ, as functions of I_M. Plots of I_M versus a_{max} at constant power ratio will then be made to compare with simulation data such as that in Fig. 20.

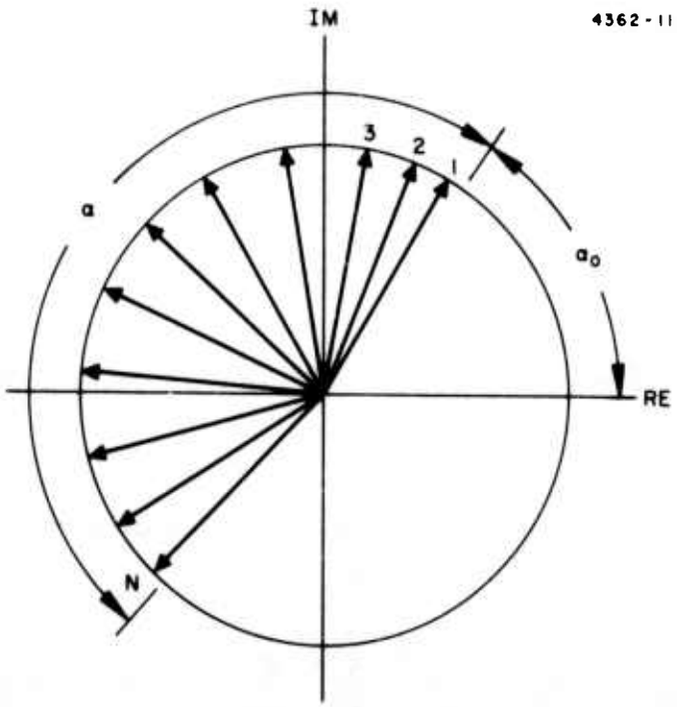

Fig. 21. Phaser diagram of a partially converged, N-element COAT array defining the quantities a and a_o used in the text.

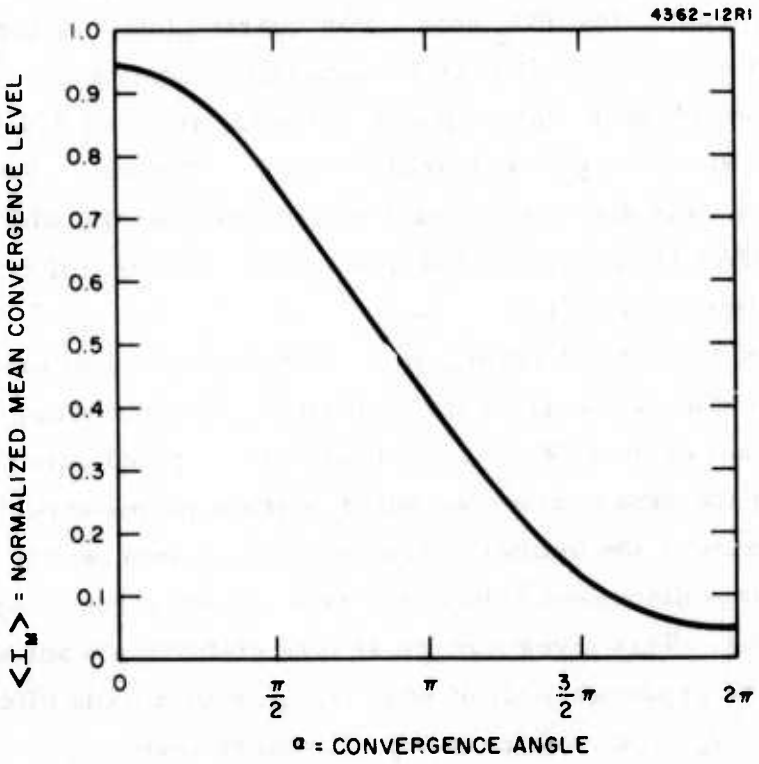

Fig. 22. Statistical expectation value of the mean convergence level, I_M, for an 18-channel multidither COAT system (dither amplitude = 20^o).

C. Thermal Blooming and Turbulence Compensation Experiments

1. Artificial Turbulence Generation

As discussed in the previous report,[1] we have chosen to use a single phase screen to produce turbulence-like effects. We have produced two phase screens by sputtering SiO_2 onto a thin quartz plate. A scan across one of these plates made by a Dektak electronic micrometer is shown in Fig. 23. The peak-to-peak optical phase variation is about 3/4 wavelength and the minimum size of a given "turbule" is about 0.5 mm. For significant turbulence effects, this diameter should be greater than the width of a single element in the COAT transmitted array, but less than the full beam diameter (five times one element width).

Because of the optical arrangement that we have been using, these plates have not produced enough beam distortion. The mounting technique produces significant beam steering, but beam breakup and scintillation is minimal. During the next quarter we will fabricate plates with "stronger" turbulence and improve the optical arrangement to maximize the effect. For the experiments discussed below, we have placed saran wrap over one of the quartz plates. This gives a more severe distortion – sometimes far too much – but also produces a lot of scattering or amplitude effects. This arrangement is being used only for our preliminary tests.

2. Flowing Gas Cell

The flowing gas cell discussed briefly in the previous report has been constructed and tested. The initial construction had several leaks which have now been eliminated. The unit, shown in Fig. 24, can produce turbulence-free air flow of up to 12 cm/sec as measured by a hot-wire anemometer; similar performance is observed with a mixture of Xenon and NO_2.

We have found it necessary to establish the absorption of this cell by direct periodic measurement rather than by filling it with a fixed NO_2 partial pressure. This is necessary because the absorption changes slowly and in an unpredictable manner as the cell runs. The cell transmission will vary as much as 30% over a two-hour period in an oscillatory manner. We do not understand this behavior, but attribute part of it to cleanup and then re-emission of the NO_2 by the sintered nickel diffuser plates in the cell.

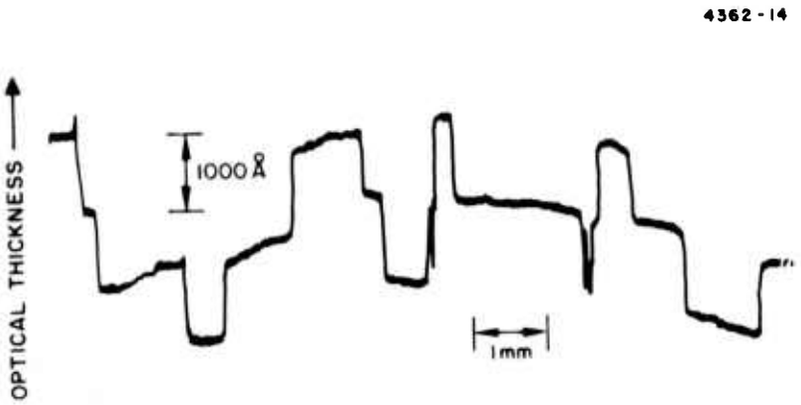

Fig. 23. Calibration scan through artificial turbulence plates using an electronic micrometer. A change in thickness of 4880 Å will produce a one wavelength phase shift for our experiments.

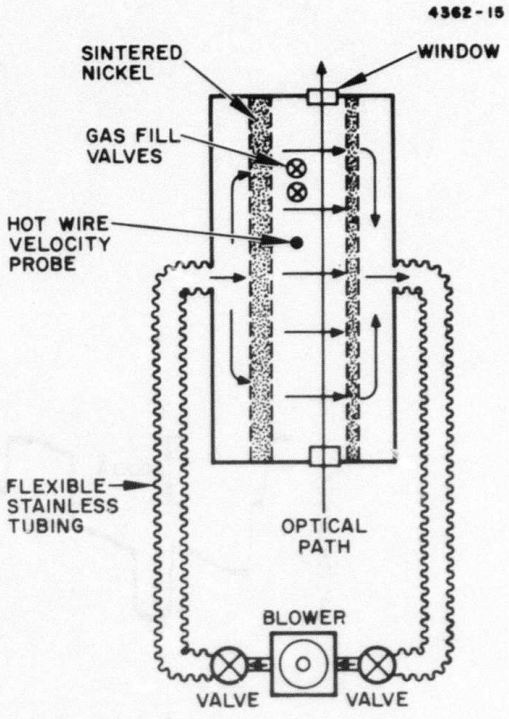

(a) Schematic drawing. Sintered nickel plates are used for diffusers to produce laminar flow.

M11189

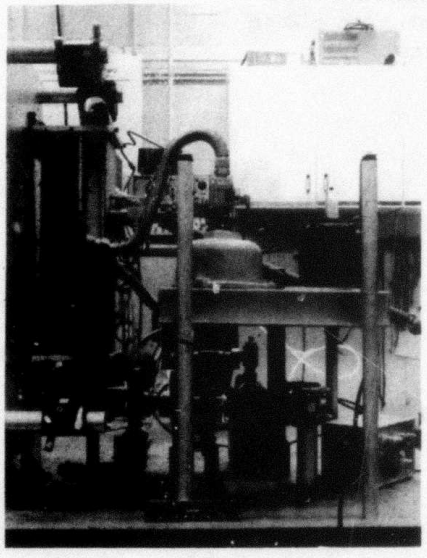

(b) Cell is mounted with a vertical path to minimize buoyancy effects.

Fig. 24. Flowing gas cell for blooming studies.

3. Blooming Compensation

Because of the initial difficulties with the flowing gas cell, we have been able to make only a few preliminary measurements of blooming compensation. We have reworked the optical arrangement now so that a 62 cm focal length lens focuses the beam through the cell. This puts the blooming in the last 81% of the propagation path. The observed results are shown in Fig. 25; previous data[1,5,6] are shown in Fig. 26 for comparison.

The data in Fig. 25 were obtained using the 18 channels of phase control and the tracking controls. The tracking controls alone produced no observable change in the peak target irradiance. They could, of course, increase the peak power on a selected glint point by steering the beam onto that point. The improvement in peak target irradiance is about 35%, still far below the factors of 2 to 3 observed with predictive phase compensation.[7,8]

We still do not understand why we see no significant compensation. It is apparent from the data in Fig. 26(a) that blooming distortions in the transmitter near field can be removed; it is equally apparent from Fig. 26(b) that those in the far field cannot be removed. It is difficult to believe that it is only the blooming in the initial 19% of the propagation path that can be compensated, but the data in Figs. 25 and 26 tend to point that way. During the next quarter we will look at two cases still of interest: (1) blooming in the first 81% of the propagation path (as opposed to the last 81% as in Fig. 25); (2) slewing beams. The second case is possible now with the tracking controls operational.

4. Turbulence Compensation

We have made some turbulence compensation studies using the artificial phase screen discussed in Section II-C-1 above. We have looked at four cases: (1) NO COAT control; (2) phase control only; (3) tracking control only; (4) phase and tracking control. The experimental arrangement is shown in Fig. 11(b) and Table I summarizes the observations. As can be seen from Table I, the phase and steering distortions in our artificial turbulence have roughly equal contributions to the uncompensated distortion.

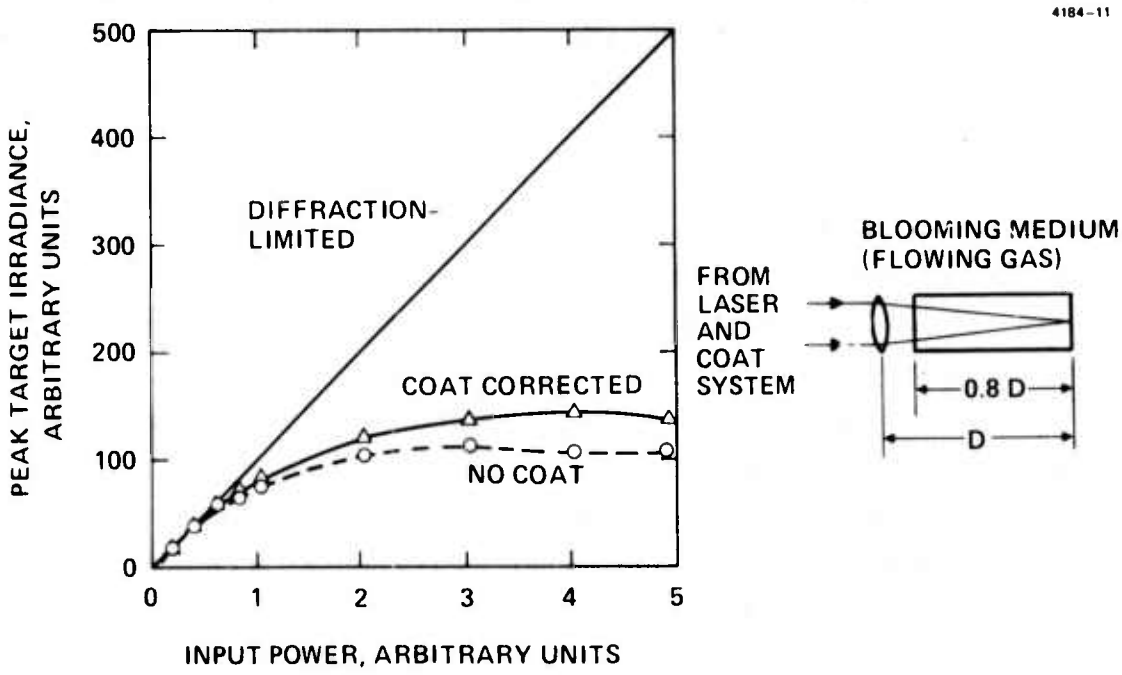

Fig. 25. Thermal blooming compensation data obtained with flowing gas cell. Also shown is the focused propagation path relative to the blooming medium.

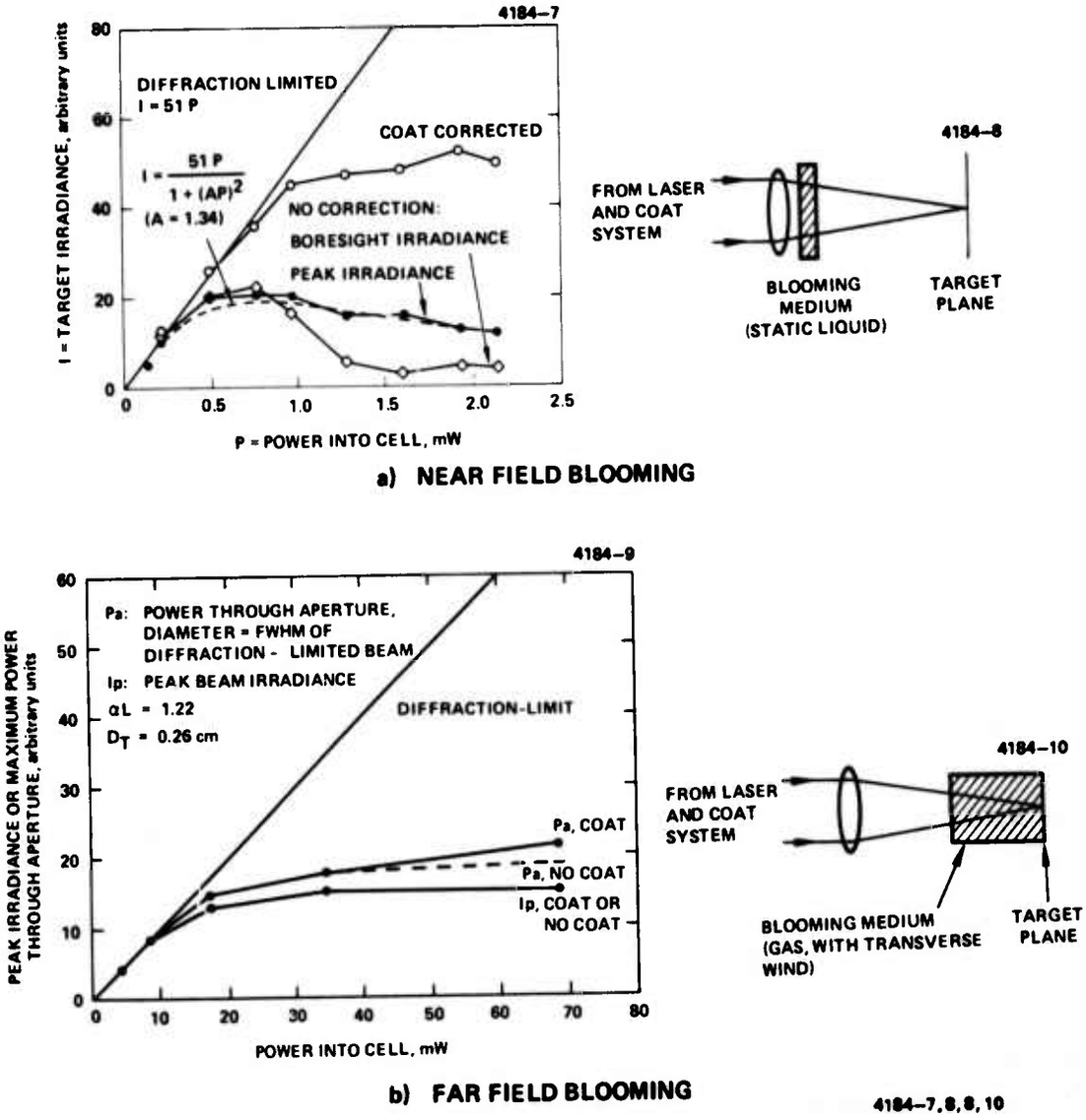

Fig. 26. Thermal blooming compensation for two propagation scenarios different from that in Fig. 25. (a) Thin static liquid cell in near-field of the transmitter. (b) Static gas cell (but transverse wind produced by mechanical motion) in last 55% of propagation path.

Table I. COAT Compensation for Artificial Turbulence

Case	Peak Target Irradiance, arb. units	Strehl Ratio,* S
NO COAT	0.39	0.65
COAT phase control	0.52	0.87
COAT tracking control	0.52	0.87
Phase and tracking control	0.57	0.95

*S = 1 is defined for no turbulence, COAT phase control.

D. Computer Simulation Results

1. Turbulence Compensation

We have demonstrated elsewhere[9,10] that the effect of atmospheric turbulence on the ensemble-averaged irradiance distribution can be accounted for by introducing a random phase screen in front of the transmitting aperture. The appropriate phase distribution is that which would be produced by a point source located on the target.* This implies that an ideal adaptive optics system should be able to completely compensate for the effects of the turbulence by introducing the conjugate phase distribution as a correction.† The degree to which this is achieved depends on whether the target has a point-glint scatterer that provides the requisite phase information and on the degree to which the adaptive optics system can reproduce the desired phase distribution.

*In this discussion, we assume that amplitude scintillation effects are small. If they are not small, the effect of atmospheric turbulence cannot be represented simply by a phase screen but rather we must also introduce a random apodization.

†Subject to the assumption that amplitude effects are negligible.

Previously[9,10] we have demonstrated that phase conjugate COAT control with a deformable mirror can correct a beam focused through a turbulent atmosphere back to within 70% to 95% of the diffraction-limited (free-space) target irradiance. We have also demonstrated analytically[10] that a multidither COAT system will arrive at the same phase correction as a phase conjugate system when correcting for linear (not power-dependent) distortions. The amount of correction depends on the range (Z), turbulence strength (C_N^2), wavelength (λ), transmitter diameter (D_T), and number of deformable corrector mirror actuators elements (N_a). The dependence of the residual phase error after correction is described by[10]

$$\langle \phi_e^2 \rangle = 0.051 \left(\frac{2\pi}{\lambda}\right)^2 C_N^2 \; Z \; D_T^{5/3} \; N_a^{-5/6} \qquad (22)$$

where $\langle \phi_e^2 \rangle$ is the residual mean square phase error across the aperture after correction. This result includes an approximation for the shape of a deformable mirror surface. The effective strehl ratio is given by

$$S \approx \exp\left[-\langle \phi_e^2 \rangle\right] \qquad (23)$$

The value of S is plotted in Fig. 28 versus C_N^2 for several cases of interest.

To provide a check on the above analytical work, we have performed two types of mirror simulations. In each, the effect of a turbulent phase screen placed in front of an aperture was compensated by a mirror with a finite number of actuators. The average Strehl ratio obtained from a sequence of five independent phase screens was determined as a function of the number of actuators. In one of the simulations the deformable mirror software was used in conjunction with a sinusoidal multidither COAT algorithm of the type used previously at HRL in our COAT servo system studies. In the other simulation, the mirror was modeled by a segmented mirror with piston and tilt control on each segment. The piston and tilt settings for each segment were determined by a least squares fit to the random phase surface over the segment.

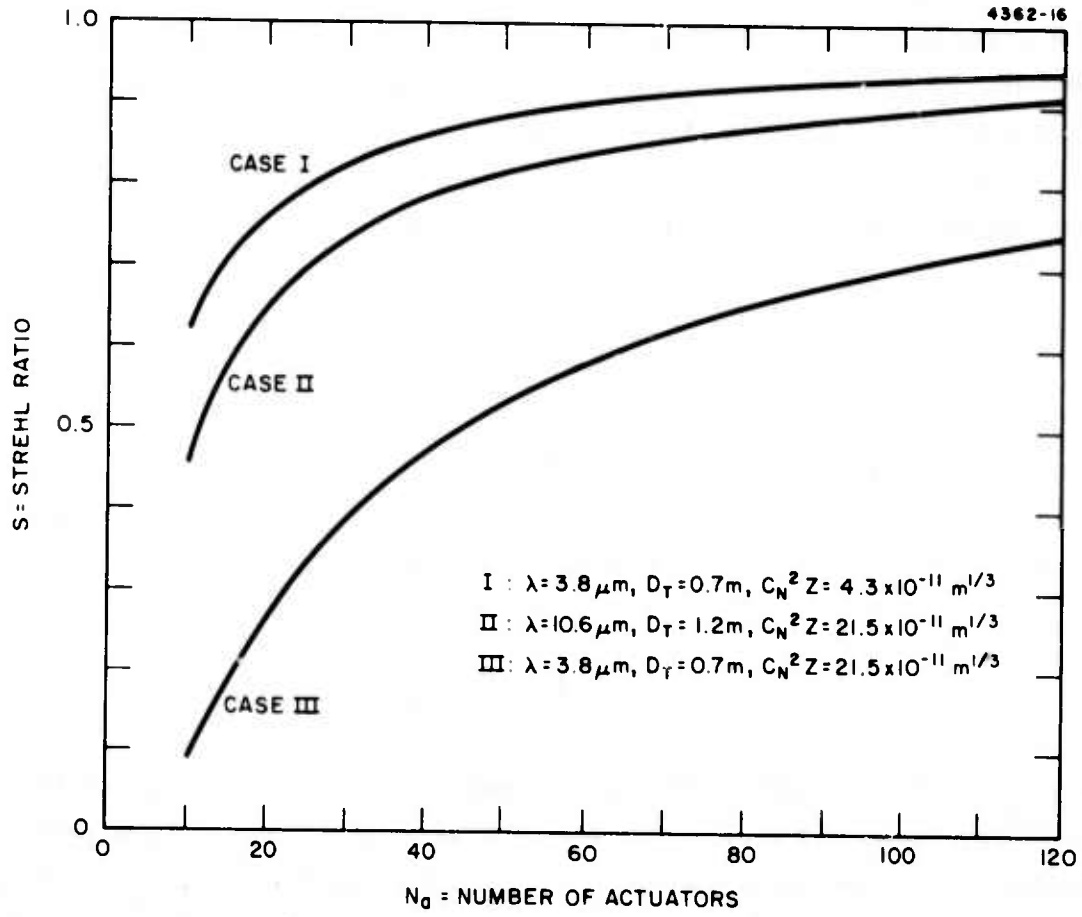

Fig. 27. Strehl ratio associated with atmospheric turbulence versus number of mirror actuators.

The agreement between the piston and tilt results and the theoretical predictions obtained from Eqs. (22) and (23) is very good (see Ref. 9 and Fig. 10 of this report), which gives us confidence in the theoretical results given in these equations. We believe that these results are representative of those that would be obtained with a deformable mirror in the absence of the $2N\pi$ problem discussed below. The results actuall obtained with a deformable mirror will depend on the degree to which the $2N\pi$ problem is avoided.

The agreement between the theory and the deformable mirror-multidither COAT simulation results is reasonably good for moderate values of C_N^2 but is poor for large values of C_N^2. We attribute the poor results obtained at large values of C_N^2 to a $2N\pi$-type of behavior. A similar problem is observed with the focus control computer simulation (see Fig. 9(b)). The deformable mirror simulation that was used in these runs has a $2N\pi$ correction loop that introduces a 2π correction whenever the phase difference between actuators exceeds four radians. The intent is to suppress 2π errors introduced by the servo system. However, if the phase distortion that is to be removed by the mirror changes by more than four radians between actuators, the 2π "correction" introduced by the $2N\pi$ correction loop is, in fact, a 2π error and the mirror performance is corresponding degraded. This problem could be avoided by removing the $2N\pi$ correction loop but then we would be faced with $2N\pi$ servo errors. One way to avoid this problem is to use more actuators so that the phase change between actuators never exceeds four radians. Another way would be to design the mirror so that the likelihood of $2N\pi$ errors is reduced, in which case the $2N\pi$ correction loop could be eliminated. More work clearly needs to be done on this problem.

2. Blooming Compensation

Although a multidither system and a phase conjugate system arrive at the same answer for linear propagation distortions, they do not reach the same result for nonlinear thermal blooming distortions. In the case of blooming, it can be demonstrated that applying the phase conjugate of a wave, generated by a point source, that propagates from the focal plane back to the transmitter does not insure maximum target irradiance: the correction

algorithm is not equivalent to a true target irradiance maximization algorithm.* A multidither algorithm, however, is a true maximization scheme (barring possible problems with 2π ambiguities).

In trying to simulate multidither compensation for blooming, we have been stopped by the lengthy computational times required. In order to accurately simulate a multidither COAT servo and blooming, a full beam propagation calculation needs to be performed at each computational increment of the servo code. This means roughtly 400 propagation computations during a single servo convergence cycle. Since each computation costs $2 to $3, the cost is prohibitive. As a result of this problem, we have performed no simulations of multidither compensation for blooming. One way to avoid this difficulty is to use a target irradiance maximization scheme rather than attempting to simulate the full multidither COAT servo. We plan on doing this in the future, but have not had the opportunity to implement such a computation on this contract.

We are beginning to accumulate evidence that the inability of a phase conjugate system to correct for blooming — and its tendency to decrease the target irradiance with strong blooming — may be common to all "return-wave" COAT systems. A return-wave COAT system is one that operates only on the wavefront returned from the target to derive the servo correction signals. Phase-conjugate systems, return-wave multidither systems,** and hybrid "TRIM-COAT" systems† are all return-wave systems. In fact, of the presently known adaptive systems, only the multidither, outgoing-wave COAT system appears to be a true maximization system.

*We have observed, as have others, that for transmitter powers exceeding the optimum power for blooming, a phase conjugate COAT correction is worse than doing nothing at all.

**The reflected coherent light sensed by the receiver is dithered, rather than the transmitted beam.

†Transmitting-Imaging: broad band, incoherent target returns are sensed by an image-compensating Imaging-COAT system and this information is used to correct the phase of the transmitted beam.

Our simulation work has also indicated that referencing off of extended target regions in the presence of blooming will give incorrect correction results. The problem is the thermal blooming equivalent of the finite isoplanatic patch size encountered in trying to image extended targets through turbulence. If the target reference region exceeds an atmospheric coherence diameter,* a COAT system will not be able to obtain the correct phase errors for the focused propagation path. We have observed during our computer simulation work with phase conjugate correction for blooming that this problem occurs even with glints less than one-half the diameter of the diffraction-limited transmitted beam on the target. We plan to study this problem further on other related programs.

*The distance between two points for which two rays from a point source see the same optical path length.

III. PLANS FOR THE NEXT QUARTER

The final contract quarter will be devoted primarily to experimental measurements. We will use the artificial turbulence generators and the flowing gas cell to look at simultaneous blooming and turbulence compensation for moving, multiple-glint targets. The performance of the 18 channels of phase control will be compared to that of just the tracking and focus controls and also the performance of all 21 channels operating simultaneously.

For the computer simulation studies, we will begin looking for techniques that will allow us to model the operation of a multidither COAT system when thermal blooming distortions are present. The speckle-noise simulation will be expanded to include additive noise effects and we will modify the code so that it can be used on the remote batch-processing facility at HRL that ties to the CDC 7600 machine at the Lawrence Berkeley Laboratories. We also plan to run some simulation cases for comparison with the acousto-optic modulation experiments discussed in this report. The analysis technique discussed in Section II-B will be used to explain the computer simulation data on speckle modulation effects.

REFERENCES

1. J. E. Pearson, "COAT Measurements and Analysis," Technical Report No. 2, Contract F30602-75-C-0001, Jan 1975; RADC-TR-75-101, May, 1975. (AD011 707)

2. M. Born and E. Wolf, Principles of Optics, Chapter 8, (Pergamon Press, 3rd Edition, 1965).

3. J. E. Pearson, M. E. Pedinoff, and S. A. Kokorowski, "Recent Advances in Multidither Coherent Optical Adaptive Techniques (COAT)" Conf. on Laser Engr. and Appl. Phys., Washington, D. C., May 1975, paper 14.9.

4. R. F. Ogrodnik and G. Gurski, "Target Return-Adaptive Aperture System Interaction Effects (U)," 1st DoD Conference on High-Energy Laser Technology, San Diego, CA Oct 1974.

5. J. E. Pearson, "COAT Measurements and Analysis," Technical Report No. 1, Contract F30602-75-C-0001, Dec. 1974; RADC-TR-75-47, Feb. 1975. (AD006 105)

6. W. B. Bridges and J. E. Pearson, Appl. Phys. Lett. 26, 539 (1975).

7. L. Bradley and J. Herrmann, Appl. Opt. 13, 331 (1974).

8. D. Fouche, unpublished.

9. W. P. Brown, Jr., Final Report, Contract N60921-74-C-0249, July 1975.

10. W. P. Brown, Jr., unpublished.

☆U.S. GOVERNMENT PRINTING OFFICE: 1975-614-357/71